NASA Contractor Report 166092

HELICOPTER ROTOR LOADS USING DISCRETIZED MATCHED ASYMPTOTIC EXPANSIONS

G. Alvin Pierce and
Anand R. Vaidyanathan

Georgia Institute of Technology
A Unit of the University System of Georgia
School of Aerospace Engineering
Atlanta, GA 30332

CONTRACT NAS1-16817

May 1983

NASA
National Aeronautics and
Space Administration

Langley Research Center
Hampton, Virginia 23665

HELICOPTER ROTOR LOADS USING DISCRETIZED MATCHED ASYMPTOTIC EXPANSIONS

By

G. Alvin Pierce

and

Anand R. Vaidyanathan

Prepared by

GEORGIA INSTITUTE OF TECHNOLOGY
SCHOOL OF AEROSPACE ENGINEERING
Atlanta, Georgia 30332

Prepared for

NATIONAL AERONAUTICS AND SPACE ADMINISTRATION
Langley Research Center
Contract NAS1-16817

Page intentionally left blank

Page intentionally left blank

CONTENTS

SUMMARY

This investigation is intended to improve the numerical practicality of a matched asymptotic expansion approach for the computation of unsteady three-dimensional airloads on a helicopter rotor. The original method as suggested by Van Holten has previously been evaluated and proven to be a comprehensive and accurate analysis for flight conditions conducive to linear flow phenomena. This effort to decrease the computational requirements of the original analysis utilizes a discretized representation of the doublet strength distribution and helical streamlines. The continuous variation of the doublet strength has been approximated by piecewise constant or piecewise quadratic distributions, and the helical trajectory of a fluid particle has been approximated by connected straight line segments. As a direct result of these simplified representations the computational time required for the execution of a typical flight condition has been reduced by an order of magnitude with respect to the requirements of the original analysis. Airloads which have been computed using the discretized method for a two-bladed model rotor and a full-scale four-bladed rotor are in close agreement with measured results and airloads from the original asymptotic analysis. For conditions characterized by significant rotor/wake interaction the piecewise constant representation requires a reduced azimuth spacing to maintain acceptable accuracy.

INTRODUCTION

The problem of estimating airloads on helicopter rotor blades can be approached by a variety of approximate methods. One such approach, put forward by Van Holten (refs. 1-4), uses an acceleration potential description of the flow field and a matched asymptotic expansion technique. Under the assumption of incompressible potential flow the unsteady three-dimensional airloads on a rotor blade in forward flight are calculated to a consistent order of approximation in terms of the aspect ratio.

A study has been conducted (ref. 5) to examine the theoretical basis and computational feasibility of the method, and to evaluate its performance and range of validity by numerical comparison with experiment and other approximate methods. The study concluded that, within the restrictions of linear theory (i.e., small disturbances), the Van Holten approach does lead to a valid description of the rotor flow field and a systematic determination of the airloads on the rotor blade. It was also found for flight conditions involving significant blade/wake interaction effects, the agreement between computation and measurement is poorer than in other cases.

The analysis in Van Holten's approach leads to an integral equation for the blade doublet strength distribution (eq. (8), ref. 5). This is solved using a collocation technique, which consists of assuming the unknown function to be made up of a combination of suitable spanwise modes and azimuthal harmonics, and satisfying the integral equation at an equal number of points distributed over the rotor disk. The result is a set of linear, simultaneous algebraic equations. However, setting up the equation at any collocation point requires integration with respect to azimuth of the individual assumed mode combinations. This numerical integration makes up the bulk of the total computation required for the solution. Under conditions of low forward speed and low inflow (when a larger azimuth range must be covered with a finer integration step) and/or a larger number of blades, the computation time is significantly increased. As an example, for a two-bladed rotor at an advance ratio of 0.3, the computer program

takes about 250 seconds to execute on a CDC 6400 computer. For other conditions, the time would vary approximately in direct proportion to the number of blades and in inverse proportion to the forward speed (advance ratio). In addition, when interaction effects are judged to be significant (possible even at moderate to high forward speeds), a smaller integration step will have to be used.

It would therefore be desirable to seek a simplified computational scheme for the basic asymptotic approach that would lead to significantly lower computation time without sacrificing any of the essential features of the asymptotic method. One possibility is to consider the analogous situation in the vortex representation of rotor wakes. In the vortex approach, the continuously varying bound circulation on the blade generates a wake in the form of a helical vortex sheet of continuously distributed trailing and shed vorticity. Calculation of the induced velocity due to such a wake would require double integration over the wake surface, which can be time-consuming. In practice, this problem is often overcome by assuming that the variation of the blade bound circulation over the span and the azimuth takes place in discrete, finite steps. This results in a wake of discrete trailing and shed vortex elements. Since the velocity induced by a straight vortex element can be analytically expressed, the induced velocity due to the entire wake can be written as a summation of analytical expressions representing the contribution of individual trailing and shed vortex elements. This results in considerable reduction of computational time over the exact numerical integration.

It appears that a similar simplification could be achieved by approximating the continuous variation of the doublet strength distribution in the asymptotic approach. It is the purpose of the current study to develop a discretized representation for the asymptotic method and compare its performance with the original computational scheme and its results with measured data for the flight conditions considered in reference 5. This report describes the details of the simplified scheme and discusses the computational results. Detailed analytical expressions are presented as Appendices.

SYMBOLS

A	aspect ratio
a_o	coning angle
a_1, b_1	blade flapping coefficients
B	number of blades
b, c	semi-chord and chord, repsectively
c_{1j}, c_{2j}, c_{3j}	coefficient of piecewise quadratic representation (eq. (A1))
d	distance between fluid particle and collocation point
d_0, d_1, d_2	coefficients of quadratic expression for d^2 in terms of θ
d_n	distance between fluid particle and point on the chord at the same spanwise location
d_{n0}, d_{n1}, d_{n2}	coefficients of quadratic expression for d_n^2 in terms of θ
F_2, F_3	terms appearing in the regular part of the near field solution (eq. (E 5))

$G_j^o, G_{jn}^c, G_{jn}^s$	harmonic coefficients in the Fourier expansion of g in terms of Ψ_b (eq. (E 1))
g	function representing the doublet strength distribution along the blade, and the basic unknown in the problem
g_j	value of g at the beginning of the j^{th} spanwise segment
I_i^c	i^{th} integral expression for the common part, Appendix B
I_i^f	i^{th} integral expression for the far field, Appendix B
I_i^n	i^{th} integral expression for the near field, Appendix B
L	total lift on one blade (eq. (E 10))
ℓ	lift per unit span, sectional lift, (eq. (E 7))
M	moment of lift distribtuion about the rotor hub (eq. (E 11))
m	sectional pitching moment about quarter-chord, positive nose-down (eq. (E 8))
p	perturbation pressure
R_0, R_1	root and tip radius of blade, respectively
R_i, R_s	coefficients of linear expression for r_b in terms of θ (eq. (B 2))
r	radial distance between fluid particle and collocation point, $\sqrt{x_b^2 + y_b^2}$
r_b	spanwise location of fluid particle
r_{bo}	spanwise location of collocation point
r_0, r_1, r_2	coefficients of quadratic expression for r^2 in terms of θ
r_j	midpoint of j^{th} spanwise segment
s	blade spanwise coordinate
s_j	spanwise location of the beginning of the j^{th} spanwise segment
Δs_j	length of j^{th} spanwise segment
U_T	local effective freestream speed
v_{io}	simple momentum induced velocity
w	induced velocity component in the z direction
Δw	incremental contribution to w
x,y,z x_b, y_b, z_b	rotor coordinate systems (fig. 1)

x_{cp}	chordwise location of center of pressure (eq. (E 9))
X_i, X_s	coefficients of linear expression for x_b in terms of θ (eq. (B 2))
Y_i, Y_s	coefficients of linear expression for y_b in terms of θ (eq. (B 2))
γ	blade inertia coefficient for flapping (Lock number)
ϵ	linear blade twist, root pitch angle-tip pitch angle
θ	azimuth position with respect to reference blade, $(\Psi_b - \Psi_{bo})$
θ_o	collective pitch angle at blade root
λ	nondimensional rotor inflow, $\mu\alpha_r + v_{io}$
μ	nondimensional rotor forward speed
ξ	R_0, R_1
ρ	air density
ϕ, η	plane elliptic coordinates
χ	meridional angle in cylindrical coordinates
Ψ_b	azimuth position with respect to downwind reference line
Ψ_{bo}	azimuth position of collocation point
$\Delta\Psi_j$	azimuth separation of j^{th} blade from reference blade
Ω	rotor angular velocity

DISCRETIZED ASYMPTOTIC REPRESENTATION

The essential features of the asymptotic approach are retained in the discretized representation, i.e., the blade pressure field is obtained in composite form as the sum of far field, near field and common part expressions in such a way that the composite field reduces to the near and far field solutions in the near and far field regions, respectively. In view of the approximations being considered, it is not known if it would be consistent to retain the terms of $O(1/A^2)$ that are present in Van Holten's analysis (ref. 1). For the sake of simplicity in computation these terms are dropped in the present study,so that the discretized representation is of $O(1/A)$, comparable to standard lifting-line formulations.

The approximations to be introduced are:

(1) The continuous variation of the unknown blade doublet strength distribution over the range of blade span and azimuth is replaced by simple, piecewise continuous functions over suitable subintervals of span and azimuth.

(2) The helical trajectory of a freestream fluid particle relative to the blade is replaced by a series of connected straight line segments.

Over the azimuth, the doublet strength variation is assumed to be piecewise constant, i.e., its value is constant over each subinterval of azimuth. Over the span, it is approximated by a piecewise constant or a piecewise quadratic variation, the latter providing a more accurate spanwise representation at the cost of more complicated algebra. Appendix A describes the manner in which these representations are

formulated, while typical representations are illustrated in figures 2(a) and 2(b).

The basic problem is the calculation of the vertical velocity induced on the blade by its pressure field, as given by the relation

$$w = -\int_{-\infty}^{\Psi_{bo}} \frac{\partial p}{\partial y_b} \, d\Psi_b \qquad (1)$$

The rotor coordinate systems are shown in figure 1 and Ψ_{bo} is the azimuth position of the reference blade. The blade pressure field is written in composite form as

$$p = p_{far} + p_{near} - p_{common}$$

By appropriate construction and matching (ref. 1), all three components can be expressed in terms of the doublet strength distribution along the lifting line.

In Van Holten's analysis, the far pressure field is the field of a dipole line along the quarter-chord location and is expressed as a series of associated Legendre functions in terms of prolate spheroidal coordinates. The near pressure field is the local two-dimensional field of the section and is expressed in plane elliptic coordinates. The common part corresponds to the behavior of the far field solution in the near field or, equivalently, that of the near field solution in the far field. With the form of the pressure field established, the induced velocity is calculated by numerical integration of the composite pressure gradient, for which purpose the above expressions are convenient. In fact, one of the merits of Van Holten's approach is that the composite pressure field is given by a direct expression free of integrals, so that the induced velocity calculation requires only one numerical integration.

However, these expressions are not convenient for the purpose of applying the proposed approximations. To O(1/A), the far field is the field of a dipole line along the blade midchord location, and can be written as the spanwise integral of a distribution of three-dimensional doublets. If the approximations described above are introduced, it is found that the calculation of the induced velocity due to the far field reduces to a double summation (over spanwise and azimuthal segments) of fairly simple integrals that can be analytically evaluated. Likewise, the near field is written as the integral, over the chord, of a two-dimensional doublet distribution, of strength proportional to the surface pressure differential. The chord is divided into a suitable number of segments over each of which the pressure differential is assumed constant, at its average value on that segment. With this simplification, the induced velocity due to the near field also becomes a double summation (over chordwise and azimuthal segments) of analytical expressions. The contribution of the common part, which is the field of a single two-dimensional dipole, presents no problems. The complete details of the various steps pertaining to the above calculations are presented in Appendices B and C. Appendix B describes the result of approximating the trajectory and also presents a list of integral expressions to be used for the induced velocity calculation. Appendix C derives the summation expressions for the induced velocity due to the far field, common part, and near field, for both the piecewise constant and the piecewise quadratic representation of the doublet strength variation along the span. Appendix C also demonstrates that the expressions derived for the far field and the common part correctly cancel in the vicinity of the blade, thus verifying their asymptotic character.

In summary, the effect of the discretized representation on the problem is to reduce the induced velocity integration of equation (1) to a summation of analytical

expressions. The normal velocity boundary condition is then applied by setting this induced velocity equal to the normal velocity on the blade surface due to blade motion. The form of this equation is given in Appendix E (eq. (E 2)). The unknowns to be solved for are the discrete values of the doublet strength at the spanwise segment midpoints, at discrete azimuth locations. However, for final presentation as output, the discrete variation with azimuth would have to be fitted by an interpolation curve. This is accomplished by substituting into equation (E 2), for the azimuth variation of each midpoint value, a harmonic interpolation formula given by (E 3). It must be noted that this does not imply a continuous azimuthal variation in the induced velocity calculation, since the doublet strength is still held constant over each azimuth segment. The advantage of the substitution is that the interpolation coefficients are obtained directly and available for calculation of output data at desired azimuth locations. Expressions for the various quantities calculated for presentation as output are given in Appendix E.

Examination of equation (E 2) shows that the near field induced velocity contains a contribution from the regular solution, proportional to the blade motion parameters. If these parameters are considered known, this contribution should be taken together with the blade normal velocity term. However, if any or all of the blade motion parameters (collective pitch, coning angle, cyclic pitch coefficients) are considered unknown, additional equations must be generated to solve for them. This can be done by using the following conditions:

(1) Azimuth average of the total lift due to all blades should equal the known rotor thrust.

(2) Flapping moment equilibrium should exist about the rotor hub.

If only first harmonic flapping is considered, the second condition yields three equations (zeroth harmonic, first harmonic cosine and first harmonic sine components). These additional equations are also listed in Appendix E, for the piecewise constant and piecewise quadratic representations.

DISCUSSION OF RESULTS

The discretized representations which have been incorporated in the analysis have been numerically evaluated to ascertain their potential accuracy. All analytical details of this evaluation are presented in Appendix D. Figure 2 illustrates the piecewise constant and quadratic representations of the spanwise distribution of doublet strength for a typical condition.

For the near field chordwise approximation, an airfoil with a steady two-dimensional pressure distribution is considered. The induced vleocity of a fluid particle travelling parallel to the chord is calculated for various vertical distances from the airfoil. The calculation is performed using both the exact solution and the approximation. The results are tabulated in Appendix D (table D1) and plotted in figure 3. It can be seen that the approximations with three segments and five segments across the chord are acceptably close to the exact solution, even at very small vertical distances. This simple example shows that, as far as the induced velocity calculation is concerned, even a relatively crude representation of the surface pressure distribution is sufficient.

For the spanwise approximations of the far field solution, a finite wing is considered with a spanwise distribution of a form which is typical of a rotor blade distribution. The induced velocity due to this distribution is calculated for a fluid particle travelling parallel to the chord, at various spanwise locations and vertical distances. The calculation is performed using the exact solution as well as the piecewise constant and piecewise quadratic approximations with three and five

spanwise segments. The results are tabulated in Appendix D (tables D2 and D3) and plotted in figure 4. With the three segment model, it can be seen that both approximations deviate from the exact solution when close to the wing, the deviations being more marked near the loaded tip and generally greater for the piecewise constant representation. With five segments, the piecewise quadratic representation is nearly identical to the exact solution while the piecewise constant results still show significant deviation very close to the wing. It may be noted that the exact and approximate results tend to merge with increasing distance from the wing, as is to be expected. It may also be noted that the results for different spanwise locations tend to merge with increasing vertical distance.

Airload computations have been carried out for the same experimental cases considered in reference 5, viz, (1) a two-bladed teetering model rotor at forward speed/tip speed ratios (μ) of 0.08, 0.15, 0.29 (ref. 6), (2) a four-bladed articulated full-scale rotor tested in flight, at μ =0.06, 0.13, 0.29 (ref. 7), and (3) the same four-bladed rotor tested in a wind tunnel at μ = 0.29, 0.39, 0.45 (ref. 8). The geometric and flight conditions are listed in table 1, which is reproduced from reference 5. The measured results are compared with computations using the piecewise constant (p.c.) and piecewise quadratic (p.q.) representations, as well as Van Holten's computational scheme. Before proceeding with a discussion of these comparisons, some comments regarding the computations are in order. In the original scheme, the numerical integration is carried out with a 5-point Gauss-Chebyschev rule over a suitable subinterval of azimuth, to be properly chosen for accurate computation. In the discretized representation, there is no numerical integration but a choice has to be made with regard to a suitable azimuth subinterval over which the trajectory is straightened. In both cases, the smaller the azimuth subinterval chosen, the more exact are the computations. In order to keep the computation economical and at the same time achieve some of the accuracy of small azimuth spacing, the procedure adopted is to use a "normal" spacing whenever the fluid particle is not close to the blade and a "reduced" spacing whenever it is close to a blade. Reference to figure 1 shows that the trajectory locations at which the fluid particle is directly over a blade are characterized by $x_b = 0$. For each collocation point (r_{bo}, Ψ_{bo}) these azimuth positions are determined in advance using equation (B 1). During the azimuth integration (or summation), a reduced spacing is used in the vicinity of these locations. In the computations carried out here (unless otherwise mentioned) the normal and reduced azimuth intervals used were 15^o and 5^o for the Van Holten scheme and 30^o and 10^o for the discretized representation. Although results of computing with the original scheme were reported in reference 5, these results were recomputed for the present study using normal and reduced spacing as above, and with spanwise collocation points at r/R_1 = 0.30, 0.55, 0.75, 0.85, 0.95. Due to these changes, some differences will be noted between the curves presented here and the corresponding ones in reference 5, but the differences are generally small with one exception which will be pointed out later on. For the discretized representation five spanwise segments were used, with end points at $r/R_1 = R_0/R_1$, 0.5, 0.7, 0.8, 0.9, 1.0, and five chordwise segments with end points at x/b = - 1.0, - 0.9, - 0.6, 0.0, 0.5, 1.0.

Results for the variation of total blade lift as a function of azimuth position for Case 1 are shown in figure 5. It can be seen that for all three forward speeds, the results of the discretized representation are quite close to the original scheme, with the p.q. representation being generally a little closer than the p.c. representation.

For Case 2, the results are illustrated in figure 6 and, as may be anticipated from the computations reported in reference 5, there is greater variation here, mainly for μ = 0.13 and μ = 0.29. At μ = 0.13, the original scheme results in a considerably wavy

TABLE I. - GEOMETRIC AND FLIGHT CONDITIONS FOR THE EXPERIMENTAL CASES

Case	Aspect ratio, A	Number of blades, B	Root Ratio, R_o/R_1	Linear twist, ε, deg.	Rotor angle, α_r, deg.	Thrust coefficient, C_T	Lock number, γ	Advance Ratio, μ	Wake Spacing, $\frac{2\pi w_r}{\Omega B R_1}$
1 (ref.21)	5.4	2	0.17	0	0	0.00367	-	0.08	0.069
					2.0	0.00482	-	0.15	0.067
					6.7	0.00394	-	0.29	0.128
2 (ref. 22)	17.2	4	0.16	8	0	0.00499	11.4	0.06	0.055
					0.6	0.00501	11.4	0.13	0.032
					6.1	0.00571	9.6	0.29	0.064
3 (ref. 23)	17.2	4	0.16	8	5.0	0.00357	10.0	0.29	0.049
					4.0	0.00366	9.9	0.39	0.050
					4.8	0.00334	10.1	0.45	0.065

distribution which is not seen in the results of the discretized scheme, especially with the p.q. representation which remains close to the measured curve except near the advancing blade position. At $\mu = 0.29$, there is once again a deviation near the advancing blade position, with the p.c. results being particularly bad in this region. The p.q. results are generally close to the original ones. However, both results from the discretized scheme tend to overestimate the lift in the disk trailing edge region (around $\Psi_b = 0^o$).

The results for Case 3 are presented in figure 7. It was observed in reference 5 that the original results showed a tendency to overestimate the lift near the downwind azimuth position and correspondingly underestimate it near the upwind position. This tendency is also present in the results from the discretized representations. This may be due to the increasingly important effect of radial flow (along the blade span) in these regions at moderate to high forward speeds. The influence of radial flow is primarily on the spanwise development of the blade boundary layer, increasing with forward speed, and must be accounted for empirically. Otherwise, the p.q. results are acceptable and show the same trend as the measured curves. However, the p.c. results show particularly significant deviations for $\mu = 0.29$ and $\mu = 0.39$, near the advancing blade position and in the disk trailing edge region. It was noted earlier that the changes made in the original scheme produced only small variations with one exception. This exception is $\mu = 0.39$ of Case 3. Comparison of figure 19 of reference 5 with figure 7(b) of the present study reveals that the latter variation is much better, particularly in the absence of the large peak near the disk trailing edge that is present in the former. This difference is surprising, at first glance, because the changes made do not seem that important. Apart from using a constant azimuth spacing, the original version of the computational scheme also used spanwise collocation points at $r/R_1 = 0.40, 0.55, 0.75, 0.85, 0.95$, differing from the present version only in the innermost point. Both programs use the zero lift condition instead of the normal velocity boundary condition at a collocation point whenever the local effective freestream speed $U_T < 0.1$. However, if $r/R_1 = 0.4$ is used, there is a collocation point near the retreating blade position that has $U_T = 0.105$, which is small yet large enough to escape the zero lift condition. It is apparently this particular point that is the source of the trouble, for when it is replaced by another collocation point with $U_T > 0.2$, the resulting distribution is quite regular (like figure 7(b) of the present study). This situation does point out the need to use care in the choice of collocation points (avoiding those points with small positive values of U_T) and use of close azimuth spacing in those cases where interference effects are significant.

Spanwise distributions of sectional lift, at various azimuth positions, are plotted in figure 8 for $\mu = 0.29$ of Case 1, and in figure 9 for $\mu = 0.29$ of Case 2. General comments on these curves are much the same as those made for the original scheme in reference 5. Agreement is acceptable as long as the measured curves do not show any sharp variations, as in the case of close interaction with a tip vortex. When sharp variations do occur, they are not evident in the computed curves. There is also general deviation from the measured curves in the tip region. In addition, the falloff to zero at the tip is better with the piecewise quadratic represenation, presumably because it provides a better approximation to the actual curve than the piecewise constant representation.

In discussing the total lift variations it was noticed that the p.c. representation led to particularly significant deviations for three flight conditions , viz, $\mu = 0.29$ of Case 2, $\mu = 0.29$ and $\mu = 0.39$ of Case 3. To test the possibility of improvement with smaller azimuth spacing, these three cases were computed again with a constant

azimuth subinterval of 5° and the results are shown plotted in figures 10 to 12. It can be seen that there is considerable improvement in the results for the p.c. representation, while the p.q. results are only slightly changed. This is a clear indication that, for flight conditions involving significant interaction effects, the results from the p.c. representation are sensitive to the azimuth spacing used and should be calculated with a small spacing.

Since the primary objective of this investigation is to improve the numerical practicality of the original asymptotic execution time requirements, it is essential that these requirements be examined. Table 2 presents results suitable for comparison of the different representations for two typical rotor configurations. In addition to the original continuous representation suggested by Van Holten and the piecewise constant and quadratic representations of this study, there is also presented data for the segmented lifting line model with a discrete vortex wake. This was the only linear method considered in reference 5 which provided airloads of an accuracy which could be compared with the asymptotic method. It can be observed from table 2 that the piecewise constant representation reduces the execution time requirement of the original continuous representation by a factor of seven. A reduction to almost one fifth is attained for the piecewise quadratic simulation. As indicated in the table, these figures are based on computational azimuth intervals of 30° normal and 10° reduced spacing. In cases where much shorter intervals are required for the piecewise constant representation the computational requirements are proportionately increased as illustrated in Table 2. It should be noted that the computational efficiency of the piecewise constant representation is equivalent to the less comprehensive segmented lifting line with a discrete vortex wake when the azimuth intervals are the same.

TABLE 2. - COMPARATIVE COMPUTER EXECUTION TIMES FOR TYPICAL CONDITIONS

Computational azimuth intervals, normal/reduced	Method of analysis	CDC 6400 execution time, sec
Case 1 $\mu = 0.29$		
$15^{\circ}/5^{\circ}$	Original continuous	231
$30^{\circ}/10^{\circ}$	Discrete vortex wake	30
	Piecewise constant	33
	Piecewise quadratic	49
Case 2 $\mu = 0.29$		
$15^{\circ}/5^{\circ}$	Original continuous	467
$30^{\circ}/10^{\circ}$	Discrete vortex wake	60
	Piecewise constant	65
	Piecewise quadratic	100
$5^{\circ}/5^{\circ}$	Discrete vortex wake	265
	Piecewise constant	265
	Piecewise quadratic	415

CONCLUDING REMARKS

The asymptotic approach developed by Van Holten is a suitable method for rotor airload calculation, within the scope of linear theory. However, in spite of the fact that only a single numerical integration is required to calculate the induced velocity, significant computation times may be required under certain conditions. It is possible to reduce the computation time by making two approximations, viz, replacing the continuous variation of the doublet strength distribtuion along the blade span by a piecewise continuous variation, and replacing the continuous helical trajectory of a fluid particle by a succession of connected straight line segments.

In the present study, such a discretized representation has been developed for the asymptotic method, using either a piecewise constant or piecewise quadratic variation of the doublet strength along the span. Computations have been carried out for the case of a two-bladed, teetering model rotor and a four-bladed, articulated full-scale rotor, and the results compared with both measurement and the original computational scheme. In general, when interaction effects are not significant, the simplified scheme agrees well with the original results, with the piecewise quadratic representation being slightly better. When interaction effects are significant, the piecewise constant scheme yields poor results but is found to improve upon using smaller azimuth spacing, while the piecewise quadratic scheme continues to compare well with the original results. Computationally, the discretized representation shows considerable improvement over the original scheme; under conditions where interaction effects are not significant, the piecewise constant scheme requires only about one-seventh and the piecewise quadratic scheme about one-fifth of the computation time required for the original scheme.

APPENDIX A

PIECEWISE CONTINUOUS REPRESENTATIONS

The continuous variation of the dipole strength function, g, over the blade span is approximated by dividing the span into J segments and replacing the actual curve by a series of simpler curves, continuous over each segment but discontinuous at the segment boundaries. The points marking the spanwise division are labeled s_j, $j = 1,2,\ldots(J+1)$ with s_1 being the root and s_{J+1} the tip of the blade. Points r_j, $j = 1,2,\ldots J$ denote the midpoints of the segments, where the boundary condition of normal velocity is applied. The length of a segment is Δs_j, $j = 1,2,\ldots J$ and this is allowed to vary along the span, generally being chosen smaller near the tip to achieve a better representation of the rapid variation of blade loading.

The simplest representation is a constant value over each segment and this is shown in figure 2. The spanwise variation can be represented much better with a second-degree curve over each segment as illustrated in figure 2. However, setting up such a piecewise quadratic representation involves more complicated algebra, the details of which are given below.

The quadratic curve is constructed to satisfy the following requirements: (1) at the midpoint, r_j, it must have the actual functional value, $g(r_j)$, (2) at its end points, s_j and s_{j+1}, it must equal the values on the adjacent segments, (3) at its end points, it must also equal the slopes of the adjacent segments. It must be noted that, for the segments at the ends of the blade, the curve is allowed to go to zero at the root and the tip, without any constraint on the slope at these points. Since each curve requires 3 constants for its definition, a total of 3 J constants must be determined from the available conditions, which are listed below.

Number of equations for midpoint values	=	J
Number of equations for end point values (including zero values at root and tip)	=	J + 1
Number of equations for end point slopes (excluding root and tip)	=	J - 1

This adds up to a total of 3 J equations, so that it is possible to set up a piecewise quadratic approximation which is completely determinate.

The curves will have to be determined in terms of the midpoint values and segment locations. To begin with, the slope conditions are ignored and the end point values assumed known. If C_{1j}, C_{2j}, C_{3j} denote the constants for the j^{th} curve, the conditions to be satisfied are

$$C_{1j} + C_{2j}\, s_j + C_{3j}\, s_j^2 = g_j$$

$$C_{1j} + C_{2j}\, r_j + C_{3j}\, r_j^2 = g(r_j)$$

$$C_{1j} + C_{2j}\, s_{j+1} + C_{3j}\, s_{j+1}^2 = g_{j+1}$$

which can be solved to give

$$C_{1j} = 2\left[r_j s_j g_{j+1} + r_j s_{j+1} g_j - 2 s_j s_{j+1} g(r_j)\right] / \Delta s_j^2$$

$$C_{2j} = -2\left[(r_j + s_j) g_{j+1} + (r_j + s_{j+1}) g_j - 4 r_j g(r_j)\right] / \Delta s_j^2 \qquad \text{(A 1)}$$

$$C_{3j} = 2\left[g_{j+1} + g_j - 2 g(r_j)\right] / \Delta s_j^2$$

Now the slope conditions can be used to elimate the end point values g_j, $j = 1,2. \ . \ .(J+1)$. At any end point, say s_{j+1}, the equality of slopes leads to

$$C_{2j} + 2 C_{3j} s_{j+1} = C_{2,j+1} + 2 C_{3,j+1} s_{j+1}$$

which, on substitution, becomes

$$(1/\Delta s_j) g_j + 3(1/\Delta s_j + 1/\Delta s_{j+1}) g_{j+1} + (1/\Delta s_{j+1}) g_{j+2} = 4\left[g(r_j)/\Delta s_j + g(r_{j+1})/\Delta s_{j+1}\right]$$

$$\text{for } j = 1,2. \ . \ .(J-1) \qquad \text{(A 2)}$$

This tridiagonal system of (J-1) equations can be solved by the following recursive scheme, which consists basically of the forward elimination and back substitution of the Gaussian elimination method.

$$\left.\begin{aligned}
\beta_2 &= 3(1/\Delta s_1 + 1/\Delta s_2) \\
\gamma_2 &= 4\left[g(r_1)/\Delta s_1 + g(r_2)/\Delta s_2\right] \\
\beta_j &= 3(1/\Delta s_{j-1} + 1/\Delta s_{j-2}) - 1/\Delta s_{j-1}^2 \, \beta_{j-1} \\
\gamma_j &= \left\{4\left[g(r_{j-1})/\Delta s_{j-1} + g(r_j)/\Delta s_j\right]\right. \\
&\quad \left. - \gamma_{j-1}/\Delta s_{j-1}\right\} / \beta_j \qquad (j = 3, 4. \ . \ . \ , J-1)
\end{aligned}\right\} \qquad \text{(A 3)}$$

$$g_J = \gamma_J$$

$$g_j = \gamma_j - g_{j+1}/\beta_j \Delta s_j \qquad (j = J-1, J-2. \ . \ .2)$$

This determines the (J-1) end point values in terms of the J midpoint values, so that the quadratic components C_{1j}, C_{2j}, C_{3j} are completely defined. Within a segment, the function can be written as

$$g = C_{1j} + C_{2j}\, s + C_{3j}\, s^2$$

$$= 2\Big[(s - s_{j+1})(s - r_j)\, g_j + (s - s_j)(s - r_j)\, g_{j+1}$$

$$- 2(s - s_j)(s - s_{j+1})\, g(r_j)\Big] \;/\Delta\, s_j^2 \qquad \text{(A 4)}$$

Calculation of the total blade lift and the moment about the hub requires the spanwise integral of g and its moment about the hub. These integrals are given below.

Piecewise constant representation:

$$\int_{\xi}^{1} g(s)\, ds = \sum_{j=1}^{J} g(r_j)\, \Delta s_j$$

$$\int_{\xi}^{1} g(s)\, s\, ds = \sum_{j=1}^{J} g(r_j)\, r_j \Delta\, s_j \qquad \text{(A 5)}$$

Piecewise quadratic representation:

$$\int_{\xi}^{1} g(s)\, ds = \sum_{j=1}^{J} \Big[g_j + g_{j+1} + 4g(r_j)\Big]\, \Delta s_j \;/\; 6$$

$$\int_{\xi}^{1} g(s)\, s\, ds = \sum_{j=1}^{J} \Big[s_j\, g_j + s_{j+1}\, g_{j+1} + 4r_j\, g(r_j)\Big] \Delta\, s_j \;/\; 6 \qquad \text{(A 6)}$$

APPENDIX B

TRAJECTORY APPROXIMATION AND LIST OF INTEGRALS

The helical trajectory of a freestream fluid particle, ending at a collocation point $(r_{bo}/R_1, \Psi_{bo})$ on a reference blade, relative to the axes fixed to the j^{th} blade, is given by the following equations.

$$\left.\begin{aligned} x_b/R_1 &= (r_{bo}/R_1 \sin(\theta + \Delta\Psi_j) + \mu\theta \sin(\theta + \Psi_{bo} + \Delta\Psi_j) \\ y_b/R_1 &= \lambda\theta \\ r_b/R_1 &= (r_{bo}/R_1)\cos(\theta + \Delta\Psi_j) + \mu\theta \cos(\theta + \Psi_{bo} + \Delta\Psi_j) \end{aligned}\right\} \quad (B\ 1)$$

where $\theta = (\Psi_b - \Psi_{bo})$ is the azimuth relative to the reference blade position and $\Delta\Psi_j$ is the azimuth separation of the j^{th} blade from the first (reference) blade. For uniformly separated blades,

$$\Delta\Psi_j = 2\pi(j - 1)/B$$

The approximation used here divides the continuous helical trajectory into a succession of straight-line segments, each connecting the initial and final points of the helical path over a subinterval of azimuth. The coordinates of each of these trajectory segments can be written as

$$\left.\begin{aligned} x_b/R_1 &= X_i + X_s\,\theta \\ y_b/R_1 &= Y_i + Y_s\,\theta \\ r_b/R_1 &= R_i + R_s\,\theta \end{aligned}\right\} \quad (B\ 2)$$

If θ_1 and θ_2 are the ends of the azimuth interval, the intercepts and slopes are given by

$$\left.\begin{aligned} X_i &= (x_{b1} - R_1 X_s\,\theta_1)/R_1 \\ X_s &= (x_{b2} - x_{b1})/R_1(\theta_2 - \theta_1) \\ Y_i &= 0 \\ Y_s &= \lambda \\ R_i &= (r_{b1} - R_1 R_s\,\theta_1)/R_1 \\ R_s &= (r_{b2} - r_{b1})/R_1(\theta_2 - \theta_1) \end{aligned}\right\} \quad (B\ 3)$$

The integrals along the fluid particle trajectories which appear in Appendix C contain the following expressions which are written in terms of the straight-line notation as

$$r^2 = x_b^2 + y_b^2 = (r_o + 2r_1\theta + r_2\theta^2) R_1^2$$

where

$$r_o = X_i^2$$

$$r_1 = X_i X_s$$

$$r_2 = X_s^2 + Y_s^2$$

Letting $u = (s - r_b)$

$$d^2 = r^2 + u^2 = (d_o + 2d_1\theta + d_2\theta^2) R_1^2$$

where

$$d_o = X_i^2 + (s - R_i)^2$$

$$d_1 = X_i X_s - (s - R_i) R_s$$

$$d_2 = X_s^2 + \lambda^2 + R_s^2$$

$$d_n^2 = (x - x_b)^2 + y_b^2 = (d_{no} + 2d_{n1}\theta + d_{n2}\theta^2) R_1^2$$

where

$$d_{n0} = (x - X_i)^2$$

$$d_{n1} = -(x - X_i) X_s$$

$$d_{n2} = X_s^2 + Y_s^2$$

The primary advantage which has been achieved by introduction of the straight-line segment approximation for the particle trajectories is evident in the above "distance" expressions. It can be noted that they are all quadratic expressions in θ. As a direct result the integrals of the pressure gradient which are described in Appendix C can be analytically evaluated. These integral expressions are listed below as determined from reference 9. The symbolic parameter, t, is defined as

$$t \equiv d_1 + d_2\theta + d\sqrt{d_2}$$

Far field integrals:

$$I_1^f = \int \frac{d\theta}{d} = \frac{\ell n\ t}{\sqrt{d_2}}$$

$$I_2^f = \int \frac{\theta\, d\theta}{d} = \frac{d - d_1 I_1^f}{d_2}$$

$$I_3^f = \int \frac{d\ \theta}{d(d-u)} - \int \frac{d\,\theta}{d(d+u)}$$

$$= \frac{2}{|X_i\ \lambda|}\left[\tan^{-1}\left\{\frac{t + (R_s d - u\sqrt{d_2})}{|X_i\ \lambda\ |}\right\}\right.$$

$$\left. - \tan^{-1}\left\{\frac{t - (R_s d - u\sqrt{d_2})}{|\ X_i\ \lambda\ |}\right\}\right]$$

$$I_4^f = I_3^f \Big|_{y_b = y_o + \lambda\theta}$$

$$I_5^f = \int \frac{\theta\ d\ \theta}{d(d-u)} - \int \frac{\theta\ d\ \theta}{d(d+u)}$$

$$= \frac{1}{r_2}\left[\ell n\left\{\frac{d-u}{d+u}\right\} - 2R_s\, I_1^f - r_1\, I_3^f\right]$$

$$I_6^f = I_5^f \Big|_{y_b = y_o + \lambda\theta}$$

$$I_7^f = \frac{\partial\, I_4^f}{\partial\, y_o}\Bigg|_{y_o \to 0}$$

$$= \frac{2\lambda(R_s d - u\sqrt{d_2})}{t r_2\, r^2} - \frac{X_s\, I_3^f}{X_i \lambda} - \frac{2 y_b u}{t d r^2}$$

$$+ \frac{2X_s(R_s d - u\sqrt{d_2})\,(X_s\, x_b + \lambda\, y_b)}{X_i\, \lambda\, t r_2 r^2}$$

$$I_8^f = \left. \frac{\partial I_6^f}{\partial y_o} \right|_{y_o \to 0}$$

$$= \left[\frac{2R_s(\lambda d + y_b\sqrt{d_2})}{td\sqrt{d_2}} - \frac{2y_b u}{dr^2} \right.$$

$$\left. + \lambda I_3^f - r_1 I_7^f \right] \frac{1}{r_2}$$

$$I_9^f = \int \frac{\theta^2 d\theta}{d(d-u)} - \int \frac{\theta^2 d\theta}{d(d+u)}$$

$$= \left[2(s - R_i) I_1^f - 2R_s I_2^f - r_o I_3^f - 2r_1 I_5^f \right] / r_2$$

$$I_{10}^f = \int \frac{d\theta}{d(d-u)^2} + \int \frac{d\theta}{d(d+u)^2}$$

$$= \frac{1}{r^2 t X_i^2 \lambda^2 \sqrt{d_2}} \left\{ 2(d_1^2 - d_0 d_2)(d\sqrt{d_2} - R_s u) \right.$$

$$\left. + t(2u + r^2 I_3^f \sqrt{d_2}) \left[r_1 R_s + r_2 (s - R_i) \right] \right\}$$

$$I_{11}^f = \int \frac{\theta\, d\theta}{d(d-u)^2} + \int \frac{\theta\, d\theta}{d(d+u)^2}$$

$$= -(2d/r^2 + r_1 I_{10}^f + R_s I_3^f) / r_2$$

$$I_{12}^{f} = \int \frac{\theta^2 d\theta}{d(d-u)^2} + \int \frac{\theta^2 d\theta}{d(d+u)^2}$$

$$= \left[2I_1^{f} + 2(s - R_i) I_3^{f} - 2R_s I_5^{f} \right.$$

$$\left. - r_0 I_{10}^{f} - 2r_1 I_{11}^{f} \right] / r_2$$

$$I_{13}^{f} = \int \frac{\theta^3 d\theta}{d(d-u)^2} + \int \frac{\theta^3 d\theta}{d(d+u)^2}$$

$$= \left[2I_2^{f} + 2(s - R_i) I_5^{f} - 2R_s I_9^{f} \right.$$

$$\left. - r_o I_{11}^{f} - 2r_1 I_{12}^{f} \right] / r_2$$

$$I_{14}^{f} = \int \frac{\theta\, d\theta}{d(d+u)}$$

$$= \frac{\ell n[2d_2 t\,(d+u)]}{r_2} - \frac{\ell n\, t}{\sqrt{d_2}\,(\sqrt{d_2} + R_s)}$$

$$- \frac{2r_1}{r_2 |X_i \lambda|} \tan^{-1} \left\{ \frac{t - (R_s d - u\sqrt{d_2})}{|X_i \lambda|} \right\}$$

$$I_{15}^{f} = \int \frac{\theta^2 d\theta}{d(d+u)}$$

$$= \left[\theta + \frac{2X_i^2(X_s^2 - Y_s^2)}{r_2 |X_i \lambda|} \tan^{-1} \left\{ \frac{t - (R_s d - u\sqrt{d_2})}{|X_i \lambda|} \right\} \right.$$

$$+ \frac{2r_1 d_2 - (\sqrt{d_2} + R_s)[r_1 R_s + r_2(s - R_i)]}{\sqrt{d_2}\ d_2 (\sqrt{d_2} + R_s)} \ln t$$

$$\left. - \frac{2r_1}{r_2} \ln \left\{ 2d_2\, t(d+u) \right\} \right] \frac{1}{r_2}$$

$$I_{16}^{f} = \int \frac{d\theta}{d-u} + \int \frac{d\theta}{d+u}$$

$$= 2I_1^{f} + (s - R_i) I_3^{f} - R_s I_5^{f}$$

$$I_{17}^{f} = \int \frac{\theta d\theta}{d-u} + \int \frac{\theta d\theta}{d+u}$$

$$= 2I_2^{f} + (s - R_i) I_5^{f} - R_s I_9^{f}$$

$$I_{18}^{f} = \int \frac{\partial}{\partial y_b} \left[y_b \ln(d+u) \right] d\theta$$

$$= \theta \ln(d+u) + R_s I_2^{f} - r_1 I_{14}^{f} - X_s^2 I_{15}^{f}$$

Some of the above integrals are not valid for the trajectory segment which ends at the collocation point for which $X_i = 0$. For this circumstance the following integrals are used.

$$I_{19}^{f} = \int \frac{\partial}{\partial y_b}\left[\frac{y_b d}{r^2}\right] d\theta \Big|_{X_i = 0}$$

$$= \frac{\lambda^2 \ell n\, t}{r_2\sqrt{d_2}} + \frac{X_s^2 - Y_s^2}{r_2^2}\left[\sqrt{d_2}\,\ell n\, t - \frac{d}{\theta}\right.$$

$$\left. - \frac{R_s(s - R_i)}{|s - R_i|}\,\ell n\left\{\frac{d_2\theta + \sqrt{d_2}(d - |s - R_i|)}{d_2\theta + \sqrt{d_2}(d + |s - R_i|)}\right\}\right]$$

$$I_{20}^{f} = \int \frac{\partial}{\partial y_b}\left[\frac{y_b d}{r^2}\right] \theta d\theta \Big|_{X_i = 0}$$

$$= \frac{\lambda^2}{r_2 d_2}\left[d + \frac{(s - R_i) R_s\, \ell n\, t}{\sqrt{d_2}}\right] + \frac{X_s^2 - Y_s^2}{r_2^2}\left[d\right.$$

$$\left. + |s - R_i|\,\ell n\left\{\frac{d_2\theta + \sqrt{d_2}\,(d - |s - R_i|)}{d_2\theta + \sqrt{d_2}(d + |s - R_i|)}\right\} - \frac{2(s - R_i) R_s\, \ell n\, t}{\sqrt{d_2}}\right]$$

$$I_{21}^{f} = \int \frac{\partial}{\partial y_b}\left[\frac{y_b u}{r^2 d}\right] d\theta \Big|_{X_i = 0}$$

$$= \frac{d(X_s^2 - Y_s^2)}{r_2^2 \theta\,|s - R_i|} + \frac{\lambda^2\,\theta}{r_2 d(s - R_i)}$$

Common part integrals

$$I_1^c = \int \frac{d\theta}{r^2}$$

$$= \frac{1}{|X_i \lambda|} \tan^{-1} \left\{ \frac{r_1 + r_2 \theta}{|X_i \lambda|} \right\}$$

$$I_2^c = \int \frac{d\theta}{r^4}$$

$$= (r_1 + r_2\theta + r_2 r^2 I_1^c) / 2X_i^2 \lambda^2 r^2$$

$$I_3^c = \int \frac{\theta d\theta}{r^4}$$

$$= -(1 + 2r_1 r^2 I_2^c) / 2r_2 r^2$$

$$I_4^c = \int \frac{\theta^2 d\theta}{r^4}$$

$$= (r_o r^2 I_2^c - \theta) / r_2 r^2$$

$$I_5^c = \int \frac{\theta^3 d\theta}{r^4}$$

$$= (\ell n\, r - r_1 I_1^c - r_o r_2 I_3^c - 2r_1 r_2 I_4^c) / r_2^2$$

$$I_6^c = \int \frac{\theta^4 d\theta}{r^4}$$

$$= (\theta^3 - 3r_o r^2 I_4^c - 4r_1 r^2 I_5^c) / r_2 r^2$$

For the special case where $X_i = 0$

$$I_2^c \Big|_{X_i = 0} = -1 / 3r_2^2\theta^3$$

$$I_3^c \Big|_{X_i = 0} = -1 / 2r_2^2\theta^2$$

$$I_4^c \Big|_{X_i = 0} = -1 / r_2^2\theta$$

$$I_5^c \Big|_{X_i = 0} = \ell n\, \theta / r_2^2$$

$$I_6^c \Big|_{X_i = 0} = \theta / r_2^2$$

Near field integrals:

$$I_1^n = \int \frac{d\theta}{d_n^2}$$

$$= \frac{1}{\lambda |x - X_i|} \tan^{-1}\left\{\frac{d_{n1} + d_{n2}\theta}{\lambda |x - X_i|}\right\}$$

$$I_2^n = \int \frac{\theta d\theta}{d_n^2}$$

$$= (\ell n\, d_n - d_{n1}\, I_1^n) / d_{n2}$$

$$I_3^n = \int \frac{\theta^2 d.\theta}{d_n^2}$$

$$= (\theta - d_{no}\, I_1^n - 2d_{n1}\, I_2^n) / d_{n2}$$

$$I_4^n = \int \frac{\theta^3 d\,\theta}{d_n^2}$$

$$= (\theta^2 - 2d_{no}\, I_2^n - 4d_{n1}\, I_3^n) / 2d_{n2}$$

APPENDIX C

INTEGRATION OF PRESSURE FIELD

The composite pressure field of the blade, to O(1/A), can be written from equations (6) and (7) of reference 5 as

$$\frac{p}{\rho\Omega^2R_1^2} = \left[\frac{p_{dip}}{\rho\Omega^2R_1^2}\right] + \left[\frac{(1-\xi)}{2A}\ \frac{g}{\rho\Omega^2R_1^2}\ \frac{\sin\chi}{r/R_1}\right] + \left[-\frac{g}{\rho\Omega^2R_1^2}\ \frac{\sin\phi}{\cosh\eta+\cos\phi}\right.$$

$$\left. + \frac{(1-\xi)}{2A}\left(F_2 + (r_b/R_1)\,F_3\right)e^{-\eta}\sin\phi\right]$$

for points within the blade span, and for points outside the span

$$\frac{p}{\rho\Omega^2R_1^2} = \frac{p_{dip}}{\rho\Omega^2R_1^2} \qquad \text{(C 1)}$$

The corresponding sectional lift is

$$\frac{\ell}{\rho\Omega^2R_1^3} = -\frac{\pi(1-\xi)}{A}\left[\frac{g}{\rho\Omega^2R_1^2} - \frac{(1-\xi)}{4A}\left(F_2 + (r_b/R_1)\,F_3\right)\right] \qquad \text{(C 2)}$$

The integration of the far field, common part and near field terms (bracketed separately on the right hand side of equation (C 1) above) will be discussed for the piecewise constant and piecewise quadratic schemes.

Far Field

To O(1/A), this is the field of a dipole line located along the blade midchord and can be expressed as the integral of point dipoles distributed along the line.

$$\frac{p_{dip}}{\rho\Omega^2R_1^2} = \frac{y_b/R_1}{4\pi}\int_{\xi}^{1}\frac{\ell}{\rho\Omega^2R_1^3}\,\frac{d(s/R_1)}{(d/R_1)^3}$$

$$= -\frac{(1-\xi)}{4A}(y_b/R_1)\int_{\xi}^{1}\frac{g}{\rho\Omega^2R_1^2}\,\frac{d(s/R_1)}{(d/R_1)^3} \qquad \text{(C 3)}$$

where $d^2 = x_b^2 + y_b^2 + (s - r_b)^2$. Using integration by parts, this can also be written as

$$\frac{p_{dip}}{\rho \Omega^2 R_1^2} = \frac{(1-\xi)}{4A} \frac{(y_b/R_1)}{(r/R_1)^2} \int_{\xi}^{1} \frac{\partial}{\partial s} \left(\frac{g}{\rho \Omega^2 R_1^2} \right) \frac{(s - r_b) ds}{d} \qquad \text{(C 4)}$$

provided g goes to zero at the root and tip. The azimuth variation of g is approximated by a piecewise constant variation over each sub-interval of azimuth, while the spanwise variation is represented by a piecewise constant or a piecewise quadratic variation, as discussed in Appendix A.

Piecewise constant representation. -

$$p_{far} = -\frac{(y_b/R_1)}{4A} (1-\xi) \sum_{j=1}^{J} g_j \int_{s_j/R_1}^{s_{j+1}/R_1} \frac{d(s/R_1)}{(d/R_1)^3}$$

$$= -\frac{(y_b/R_1)}{4A} \frac{(1-\xi)}{(r/R_1)^2} \sum_{j=1}^{J} g_j \left[\frac{s - r_b}{d} \right]_{s=s_j}^{s=s_{j+1}}$$

The function g_j which varies with azimuth will have a constant value over the i^{th} azimuth subinterval that will be denoted by g_{ij}. The velocity induced by the far field is given by

$$\frac{w_{far}}{\Omega R_1} = \frac{(1-\xi)}{4A} \sum_i \sum_j g_{ij} \int_{\theta_{i+1}}^{\theta_i} \frac{\partial}{\partial (y_b/R_1)} \left[\frac{(y_b u)/R_1^2}{(r^2 d)/R_1^3} \right] d\theta \Bigg|_{s_j}^{s_{j+1}} \qquad \text{(C 5)}$$

where $u = s - r_b$. The integration will be easier if the derivative can be taken out of the integral and this is done as,

$$\frac{w_{far}}{\Omega R_1} = -\frac{(1-\xi)}{4A} \lim_{y_o \to 0} \frac{\partial}{\partial (y_o/R_1)} \sum_i \sum_j g_{ij} \int_{\theta_{i+1}}^{\theta_i} \frac{(y_b - y_o) u/R_1^2}{(r^2 d)/R_1^3} d\theta \Bigg|_{s_j}^{s_{j+1}}$$

where now $d^2 = x_b^2 + (y_b - y_o)^2 + u^2$. Noting that

$$\frac{u}{r^2 d} = \frac{1}{2} \left[\frac{1}{d(d-u)} - \frac{1}{d(d+u)} \right]$$

the integration can now be evaluated using the integrals listed in Appendix B with $y_b/R_1 = \lambda\theta$, where λ is the inflow ratio.

$$\int_{\theta_{i+1}}^{\theta_i} \frac{(y_b - y_o)\, u/R_1^2}{(r^2 d)/R_1^3}\, d\theta = -\frac{y_o}{R_1} I_4^f + \lambda I_6^f \Bigg|_{\theta_{i+1}}^{\theta_i}$$

Carrying out the differentiation and letting $y_o \to 0$, the induced velocity is obtained as

$$\frac{w_{far}}{\Omega R_1} = \sum_i \sum_j (\Delta w_{far})_{ij}^{p.c.}\, g_{ij} \qquad (C\ 6)$$

where, for $i \neq 1$,

$$(\Delta w_{far})_{ij}^{p.c.} = -\frac{(1-\xi)}{4A}\left(-I_4^f + \lambda I_8^f\right)\Bigg|_{\theta_{i+1}}^{\theta_i}\Bigg|_{s_j}^{s_{j+1}}$$

Here, the azimuth index i is set up so that $\theta_1 = 0$ is the collocation point on the blade and the trajectory ranges over $-\infty < \theta \leq 0$. For $i = 1$, the trajectory segment has one end on the blade and the unit induced velocity is expressed as

$$(\Delta w_{far})_{ij}^{p.c.} = \frac{(1-\xi)}{4A} I_{21}^f \Bigg|_{\theta_2}^{\theta_1}\Bigg|_{s_j}^{s_{j+1}}$$

Piecewise quadratic representation. - For this case, it is more convenient to express the field of the dipole line in its second form (eq. (C 4)). Using the representation of Appendix A as

$$\frac{\partial}{\partial(s/R_1)}\left(\frac{g}{\rho\,\Omega^2 R_1^2}\right) = C_{2j} + 2C_{3j}(s/R_1)$$

$$\frac{p_{far}}{\rho\,\Omega^2 R_1^2} = \frac{(1-\xi)}{4A}\,\frac{y_b/R_1}{(r/R_1)^2}\sum_{j=1}^{J}\int_{s_j}^{s_{j+1}}\left\{C_{2j} + 2C_{3j}(s/R_1)\right\}\frac{uds/R_1^2}{d/R_1}$$

$$\frac{p_{far}}{\rho \Omega^2 R_1^2} = \frac{(1-\xi)}{4A} \sum_{j=1}^{J} \left[\left\{ C_{2j} + C_{3j} (r_b + s)/R_1 \right\} \frac{y_b d}{r^2} \right.$$

$$\left. - C_{3j} (y_b/R_1) \ln \left\{ (u + d)/R_1 \right\} \right]_{s_j}^{s_{j+1}}$$

The induced velocity can then be written as

$$\frac{w_{far}}{\Omega R_1} = -\frac{(1-\xi)}{4A} \sum_i \sum_j \left[(C_{2j} + C_{3j} R_i + C_{3j} s/R_1)_i \int_{\theta_{i+1}}^{\theta_i} \frac{\partial}{\partial (y_b/R_1)} \left[\frac{y_b d/R_1^2}{(r/R_1)^2} \right] d\theta \right.$$

$$+ (C_{3j} R_s)_i \int_{\theta_{i+1}}^{\theta_i} \theta \frac{\partial}{\partial (y_b/R_1)} \left[\frac{y_b d/R_1^2}{(r/R_1)^2} \right] d\theta$$

$$\left. - (C_{3j})_i \int_{\theta_{i+1}}^{\theta_i} \frac{\partial}{\partial (y_b/R_1)} \left[(y_b/R_1) \ln \left\{ (u + d)/R_1 \right\} \right] d\theta \right]_{s_j}^{s_{j+1}} \qquad \text{(C 7)}$$

It may be noted that

$$\frac{\partial}{\partial y_b} (y_b d/r^2) = (x_b^2 - y_b^2)\, d/r^4 + y_b^2 / r^2 d$$

$$= \frac{1}{2} \left[\frac{1}{d+u} + \frac{1}{d-u} - \frac{y_b^2}{d(d+u)^2} - \frac{y_b^2}{d(d-u)^2} \right]$$

Using this relation, and consulting the integrals listed in Appendix B, the induced velocity can be expressed as

$$\frac{w_{far}}{\Omega R_1} = \sum_i \sum_j (\Delta w_{far})_{ij}^{p.q.} g_i(r_j) \qquad \text{(C 8)}$$

where $g_i(r_j)$ is the midpoint value of the j^{th} spanwise segment within the i^{th} azimuth interval. In terms of the quadratic coefficients, equation (C 7) can be written for $i \neq 1$ as

$$\frac{w_{far}}{\Omega R_1} = -\frac{(1-\xi)}{4A}\sum_i \sum_j \Big[(C_{2j} + C_{3j} R_i + C_{3j} s/R_1)_i$$

$$\times (I_{16}^f - \lambda^2 I_{12}^f)/2 + (C_{3j} R_s)_i (I_{17}^f - \lambda^2 I_{13}^f)/2$$

$$- (C_{3j})_i I_{18}^f \Big] \Big|_{\theta_{i+1}}^{\theta_i} \Big|_{s_j}^{s_{j+1}}$$

and for $i = 1$ as

$$\Delta\left(\frac{w_{far}}{\Omega R_1}\right)_{i=1} = -\frac{(1-\xi)}{4A} \sum_j \Big[(C_{2j} + C_{3j} R_i + C_{3j} s/R_1)_1 I_{19}^f$$

$$+ (C_{3j} R_s)_1 I_{20}^f - (C_{3j})_1 I_{21}^f \Big] \Big|_{\theta_2}^{\theta_1} \Big|_{s_j}^{s_{j+1}}$$

The quadratic coefficients can be expressed in terms of the midpoint and end point values. In turn, the end point values can be expressed in terms of the midpoint values, as shown in Appendix A, to obtain a final expression for the unit induced velocity of equation (C 8). The expression is lengthy and will not be reproduced here.

Common Part

The common part is the pressure field to which the far field tends at points very close to the dipole line, when it behaves essentially as a two-dimensional dipole corresponding to the doublet strength at that spanwise location.

$$\frac{p_{common}}{\rho \Omega^2 R_1^2} = -\frac{(1-\xi)}{2A} \frac{y_b/R_1}{(r/R_1)^2} \frac{g(r_b,\theta)}{\rho \Omega^2 R_1^2}$$

The induced velocity due to the common part is calculated as

$$\frac{w_{common}}{\Omega R_1} = \int_{\infty}^{0} \frac{\partial}{\partial(y_b/R_1)} \left(\frac{P_{common}}{\rho \Omega^2 R_1^2}\right) d\theta \qquad (C\ 9)$$

Piecewise constant representation. - Noting that

$$\frac{\partial}{\partial y_b} (y_b/r^2) = (x_b^2 - y_b^2)/r^4$$

equation (C 9) becomes

$$\frac{w_{common}}{\Omega R_1} = -\frac{(1-\xi)}{2A} \sum_i g_{ij} \left[X_i^2 \int_{\theta_{i+1}}^{\theta_i} \frac{d\theta}{(r/R_1)^4} + 2X_i X_s \int_{\theta_{i+1}}^{\theta_i} \frac{\theta\, d\theta}{(r/R_1)^4} + (X_s^2 - \lambda^2) \int_{\theta_{i+1}}^{\theta_i} \frac{\theta^2 d\theta}{(r/R_1)^4} \right]$$

The index j represents the spanwise segment within which the i^{th} trajectory segment lies; in general, the trajectory segment may range over more than one spanwise segment, in which case the azimuth interval must be subdivided so that each of the subintervals lies entirely within one spanwise segment.

$$\frac{w_{common}}{\Omega R_1} = \sum_i (\Delta w_{common})_i^{p.c.} \; g_{ij} \qquad (C\ 10)$$

where, from Appendix B,

$$(\Delta w_{common})_i^{p.c.} = -\frac{(1-\xi)}{2A} \left[X_i^2 I_2^c + 2X_i X_s I_3^c + (X_s^2 - \lambda^2) I_4^c \right] \Bigg|_{\theta_{i+1}}^{\theta_i}$$

Piecewise quadratic representation. - The spanwise variation of g is given by equation (A 4) of Appendix A. The induced velocity is given by

$$\frac{w_{common}}{\Omega R_1} = -\frac{(1-\xi)}{2A}\sum_i \frac{2}{\Delta s_j^2}\Big[g_{ij}\Big\{(R_i - s_{j+1})(R_i - r_j)C_1$$

$$+ R_s(2R_i - r_j - s_{j+1})C_2 + R_s^2 C_3\Big\} + g_{i,j+1}\Big\{(R_i - s_j)(R_i - r_j)C_1$$

$$+ R_s(2R_i - r_j - s_j)C_2 + R_s^2 C_3\Big\} - 2g_i(r_j)\Big\{(R_i - s_j)(R_i - s_{j+1})C_1$$

$$+ R_s(2R_i - s_j - s_{j+1})C_2 + R_s^2 C_3\Big\}\Big]$$

where

$$C_1 = \Big[X_i^2 I_2^c + 2X_i X_s I_3^c + (X_s^2 - \lambda^2) I_4^c\Big]\Big|_{\theta_{i+1}}^{\theta_i}$$

$$C_2 = \Big[X_i^2 I_3^c + 2X_i X_s I_4^c + (X_s^2 - \lambda^2) I_5^c\Big]\Big|_{\theta_{i+1}}^{\theta_i}$$

$$C_3 = \Big[X_i^2 I_4^c + 2X_i X_s I_5^c + (X_s^2 - \lambda^2) I_6^c\Big]\Big|_{\theta_{i+1}}^{\theta_i}$$

Both g_{ij} and $g_{i,j+1}$ can be expressed in terms of the midpoint values, and the induced velocity can be finally written as

$$\frac{w_{common}}{\Omega R_1} = \sum_i (\Delta w_{common})_i^{p \cdot q \cdot} g_i(r_j) \qquad \text{(C 11)}$$

Near Field

The near field is a distribution of two-dimensional dipoles along the chord, of intensity proportional to the surface pressure differential.

$$\frac{p_{near}}{\rho \Omega^2 R_1^2} = \frac{y_b}{\pi R_1}\int_{-1}^{1} \frac{-\frac{g}{\rho \Omega^2 R_1^2}\sqrt{\frac{1-x}{1+x}} + \frac{(1-\xi)}{2A}\left(F_2 + (r_b/R_1)F_3\right)\sqrt{1-x^2}}{(x - x_b R_1/b)^2 + (y_b R_1/b)^2}\,dx$$

where b is the semi-chord.

To make analytical integration possible, the chord is divided into K segments and the factors $\sqrt{1-x/1+x}$ and $\sqrt{1-x^2}$ are replaced by an average value over each segment. The chordwise integration can then be carried out, resulting in

$$\frac{\partial}{\partial(y_b/R_1)}\left(\frac{P_{near}}{\rho\,\Omega^2 R_1^2}\right) = -\sum_{k=1}^{K}\frac{f_k}{\pi}\left[\frac{\left(\frac{1-\xi}{2A}\,x - x_b\right)/R_1}{\left\{\left(\frac{1-\xi}{2A}\,x - x_b\right)^2 + y_b^2\right\}/R_1^2}\right]_{x_k}^{x_{k+1}}$$

where $f_k = \frac{g}{\rho\,\Omega^2 R_1^2}\,a_k - \frac{(1-\xi)}{2A}\left[F_2 + (r_b/R_1)\,F_3\right]b_k$

$$a_k = \left.\frac{\phi - \sin\phi}{x_k}\right|_{\phi_k}^{\phi_{k+1}}$$

$$b_k = \left.\frac{\phi/2 - (\sin 2\phi)/4}{\Delta x_k}\right|_{\phi_k}^{\phi_{k+1}}$$

$$x_k = \cos\phi_k \quad ; \quad \Delta x_k = x_{k+1} - x_k$$

Piecewise constant representation. -

$$\frac{w_{near}}{\Omega R_1} = -\int_{-\infty}^{0}\frac{\partial}{\partial(y_b/R_1)}\left(\frac{P_{near}}{\rho\,\Omega^2 R_1^2}\right)d\theta$$

$$= \sum_i\sum_k\frac{f_{ik}}{\pi}\int_{\theta_{i+1}}^{\theta_i}\frac{\left(\frac{1-\xi}{2AR_1}\,x - X_i\right) - X_s\theta}{d_n^2/R_1^2}\,d\theta\Bigg|_{x_k}^{x_{k+1}} \qquad \text{(C 12)}$$

Here, the factor $[F_2 + (r_b/R_1) F_3]$ is taken to be a constant for each azimuth interval i. Using the integrals listed in Appendix A, the induced velocity can be written as

$$\frac{w_{near}}{\Omega R_1} = \sum_i \sum_k \left[(\Delta w^I_{near})^{p.c}_{ik} \; g_{ij} + (\Delta w^{II}_{near})^{p.c.}_{ik} \right] \qquad (C\ 13)$$

where

$$(\Delta w^I_{near})^{p.c.}_{ik} = \frac{a_k}{\pi} \left[\left(\frac{1-\xi}{2A} \frac{x}{R_1} - X_i \right) I_1^n - X_s I_2^n \right] \Bigg|_{\theta_{i+1}}^{\theta_i} \Bigg|_{x_k}^{x_{k+1}}$$

$$(\Delta w^{II}_{near})^{p.c.}_{ik} = - \frac{(1-\xi)}{2A} \frac{b_k}{\pi} \left[F_2 + (r_b/R_1) F_3 \right]_i$$

$$\times \left[\left(\frac{1-\xi}{2A} \frac{x}{R_1} - X_i \right) I_1^n - X_s I_2^n \right] \Bigg|_{\theta_{i+1}}^{\theta_i} \Bigg|_{x_k}^{x_{k+1}}$$

F_2 and F_3 contain terms proportional to blade motion, namely, θ_o, a_o, a_1, b_1 and the twist ε.

Piecewise quadratic representation. - Here, the quadratic expression for the variation of g over a spanwise segment is used and the induced velocity becomes

$$\frac{w_{near}}{\Omega R_1} = \sum_i \sum_k \frac{2a_k}{\pi \Delta s_j^2} \Big[g_{ij} \left\{ (R_i - s_{j+1})(R_i - r_j) n_o + R_s(2R_i - r_j - s_{j+1}) n_1 + R_s^2 n_2 \right\} + g_{i,j+1} \left\{ (R_i - s_j)(R_i - r_j) n_o + R_s(2R_i - r_j - s_j) n_1 + R_s^2 n_2 \right\} - 2g_i(r_j) \left\{ (R_i - s_j)(R_i - s_{j+1}) n_o + R_s(2R_i - s_j - s_{j+1}) n_1 + R_s^2 n_2 \right\} \Big] + \sum_i \sum_k \frac{2b_k}{\pi \Delta s_j^2} \left[F_2 + (r_b/R_1) F_3 \right]_i n_o$$

where

$$n_o = \left[\left(\frac{1-\xi}{2A}\,\frac{x}{R_1} - X_i\right) I_1^n - X_s I_2^n\right] \Bigg|_{\theta_{i+1}}^{\theta_i} \Bigg|_{x_k}^{x_{k+1}}$$

$$n_1 = \left[\left(\frac{1-\xi}{2A}\,\frac{x}{R_1} - X_i\right) I_2^n - X_s I_3^n\right] \Bigg|_{\theta_{i+1}}^{\theta_i} \Bigg|_{x_k}^{x_{k+1}}$$

$$n_2 = \left[\left(\frac{1-\xi}{2A}\,\frac{x}{R_1} - X_i\right) I_3^n - X_s I_4^n\right] \Bigg|_{\theta_{i+1}}^{\theta_i} \Bigg|_{x_k}^{x_{k+1}}$$

As before, the induced velocity expression can be symbolically written as

$$\frac{w_{near}}{\Omega R_1} = \sum_i \sum_k \left[\left(\Delta w^{I}_{near}\right)^{p.q.}_{ik} g_{ij} + \left(\Delta w^{II}_{near}\right)^{p.q.}_{ik}\right] \qquad (C\ 14)$$

Limiting Behavior

The behavior of the expressions for the far field and the common part, in the vicinity of the lifting line, will be studied for both piecewise representations.

Piecewise constant representation. - It is sufficient to look at the expressions used for the trajectory segment immediately adjacent to the collocation point on the blade, viz, the segment with i = 1. Let the collocation point be located at the center of spanwise segment m. The unit induced velocity for the far field can be written out in full as below, for i = 1 (see eq. (C 6)).

$$\left(\Delta w_{far}\right)^{p.c.}_{1j} = -\frac{(1-\xi)}{4A}\left[\frac{(X_s^2 - \lambda^2)}{r_2^2}\left(\frac{d}{\frac{s}{R_1} - R_i}\right)\theta + \frac{\lambda^2}{r^2}\left(\frac{\theta}{\frac{s}{R_1} - R_i}\right) d\right] \Bigg|_{\theta_2}^{\theta_1} \Bigg|_{s_j}^{s_{j+1}}$$

$$\text{As } \theta \to 0, \quad d \to \left|\frac{s}{R_1} - R_i\right| - R_s \frac{\left(\frac{s}{R_1} - R_i\right)}{\left|\frac{s}{R_1} - R_i\right|}\theta \ \ldots ,$$

indicating that the first term in the expansion for d will give rise to a singular term, which can be separated out.

$$\lim_{\theta \to 0} \left[\sum_{j=1}^{J} (\Delta w_{far})_{1j}^{p.c.} \; g_{1j} \right]_{sing}$$

$$= - \frac{(1-\xi)}{4A} \frac{(X_s^2 - \lambda^2)}{r_2^2} \frac{1}{\theta} \sum_{j=1}^{J} \frac{\left| \frac{s}{R_1} - R_i \right|}{\left(\frac{s}{R_1} - R_i \right)} \Bigg|_{s_j}^{s_{j+1}} g_{1j}$$

$$= - \frac{(1-\xi)}{2A} \frac{(X_s^2 - \lambda^2)}{r_2^2} \frac{1}{\theta} \; g_{1m}$$

since $R_i = r_m$. Similarly, by looking at the behavior of the common part expression for $i = 1$, it is found that (see eq. (C 10))

$$\lim_{\theta \to 0} (\Delta w_{common})_1^{p.c.} = - \frac{(1-\xi)}{2A} (X_s^2 - \lambda^2) \left(- \frac{1}{r_2^2 \theta} \right) g_{1m}$$

since $X_i = 0$. It can be seen that the two terms cancel each other exactly.

Piecewise quadratic representation. - In a manner similar to that above, the singular part of the far field expression (eq. (C 8)) can be separated out.

$$\lim_{\theta \to 0} \left[\Delta \left(\frac{w_{far}}{\Omega R_1} \right)_{i=1} \right]_{sing}$$

$$= - \frac{(1-\xi)}{4A} \frac{(X_s^2 - \lambda^2)}{r_2^2} \sum_j \left[(C_{2j} + C_{3j} R_i + C_{3j} s/R_1) \left\{ - \frac{\left| \frac{s}{R_1} - R_i \right|}{\theta} \right.\right.$$

$$\left.\left. - R_s \frac{\left(\frac{s}{R_1} - R_i \right)}{\left| \frac{s}{R_1} - R_i \right|} \ln \theta \right\} + C_{3j} R_s \left| \frac{s}{R_1} - R_i \right| \ln \theta \right] \Bigg|_{s_j}^{s_{j+1}}$$

Now, $C_{2j} = g'(r_j) - 2(r_j/R_1) C_{3j}$

Using this relation and carrying out the summation with j, it can be shown that the above limiting expression simplifies to

$$\lim_{\theta \to 0} \left[\Delta \left(\frac{w_{far}}{\Omega R_1} \right)_{i=1} \right]_{sing}$$

$$= - \frac{(1 - \xi)}{4A} \frac{(X_s^2 - \lambda^2)}{r_2^2} \left[2g(r_m) \frac{1}{\theta} - 2R_s g'(r_m) \ell n \theta \right]$$

The limiting value for the common part (eg. (C 11)) can be shown to be

$$\lim_{\theta \to 0} \left[\Delta \left(\frac{w_{common}}{\Omega R_1} \right)_{i=1} \right]$$

$$= - \frac{(1 - \xi)}{2A} \frac{(X_s^2 - \lambda^2)}{r_2^2} \left[\frac{R_s}{\Delta s_m} (g_{i,m+1} - g_{im}) \ell n \theta - g(r_m) \frac{1}{\theta} \right]$$

Since

$$g'(r_m) = (g_{i,m+1} - g_{im}) / \Delta s_m$$

it can be seen that the singularities in the far field and common part cancel exactly.

APPENDIX D

EVALUATION OF CHORDWISE AND SPANWISE APPROXIMATIONS

To facilitate the analytical integration of the pressure field in calculating the velocity induced on the blade, approximations are used for chordwise and spanwise variations, as outlined in Appendices A and C. This Appendix attempts to evaluate the accuracy of these approximations.

Chordwise Approximation

This consists of replacing the factors $\sqrt{1-x/1+x}$ and $\sqrt{1-x^2}$ by their average values over each chordwise segment. Since the first factor is the significant portion of the chordwise pressure distribution, the following problem is considered. Calculate the velocity induced by a steady, two-dimensional pressure distribution (proportional to $\sqrt{1-x/1+x}$) on a fluid particle travelling parallel to the chord, using both the exact and approximate pressure distributions.

The (x, y) axes are centered at the midchord with the x-axis being parallel to the chord. The exact nondimensional pressure field of the airfoil is given by

$$p_e(x, y) = \frac{y}{2\pi} \int_{-1}^{1} \sqrt{\frac{1-x'}{1+x'}} \frac{dx'}{(x'-x)^2 + y^2}$$

$$= \frac{1}{2} \frac{\sin \phi}{\cosh \eta + \cos \phi}$$

where (η, ϕ) is an elliptic coordinate system with

$$x = \cosh \eta \cos \phi$$

$$y = \sinh \eta \sin \phi$$

If the trajectory considered extends from x = - 2 to x = 2 at a constant distance y, the nondimensional induced velocity is given by

$$v = - \int_{-2}^{2} \frac{\partial p_e}{\partial y} dx$$

$$= - \frac{1}{2} \int_{-2}^{2} \frac{\sinh \eta \cos \phi + \sinh \eta \cosh \eta \cos 2 \phi}{(\cosh^2 \eta - \cos^2 \phi)(\cosh \eta + \cos \phi)^2} dx \qquad \text{(D 1)}$$

This integral can be evaluated by numerical integration.

Using the approximation, the average value of the pressure distribution over the k^{th} chordwise segment is given by

$$\bar{p}_k = \frac{1}{x_{k+1} - x_k} \int_{x_k}^{x_{k+1}} \sqrt{\frac{1-x}{1+x}}\, dx$$

$$= -\frac{1}{x_{k+1} - x_k} \left[\theta_{k+1} - \theta_k - \sin \theta_{k+1} + \sin \theta_k\right]$$

where $x_k = \cos \theta_k$.

$$p_e(x, y) = \frac{y}{2\pi} \sum_{k=1}^{K} \bar{p}_k \int_{x_k}^{x_{k+1}} \frac{dx'}{(x' - x)^2 + y^2}$$

$$\frac{\partial p_e}{\partial y} = -\sum_{k=1}^{K} \frac{\bar{p}_k}{2\pi} \frac{(x' - x)}{(x' - x)^2 + y^2} \Bigg|_{x_k}^{x_{k+1}}$$

$$v = \sum_{k=1}^{K} \frac{\bar{p}_k}{4\pi} \ln \left\{\frac{(x_{k+1} - x)^2 + y^2}{(x_k - x)^2 + y^2}\right\} \Bigg|_{x=-2}^{x=2} \qquad \text{(D 2)}$$

Two approximations are considered: (1) three segments along the chord, $\Delta x_k = 0.1, 0.9, 1.0$; and (2) five segments along the chord, $\Delta x_k = 0.1, 0.4, 0.5, 0.5, 0.5$. The results for the induced velocity are listed in table D 1. These results are also plotted in figure 3 and it can be seen that the approximate results are quite close to the exact results, even down to a vertical distance of 1% of the semi-chord.

TABLE D 1. - COMPARATIVE EVALUATION OF CHORDWISE APPROXIMATION

Vertical distance, y	Exact	Three segments	Five segments
.01	.5773	.5708	.5738
.05	.5766	.5702	.5731
.10	.5745	.5681	.5711
.20	.5661	.5602	.5629
.30	.5529	.5476	.5501
.40	.5357	.5313	.5335
.50	.5157	.5121	.5139
.60	.4938	.4910	.4925
.70	.4709	.4689	.4700
.80	.4476	.4464	.4472
.90	.4246	.4241	.4245
1.00	.4022	.4022	.4024

Spanwise Approximation

As discussed elsewhere, the span is divided into J segments, over each of which the variation of the function g is replaced by a piecewise constant or piecewise quadratic function. To evaluate this approximation, the following problem is considered. Calculate the velocity induced by a finite wing on a fluid particle travelling with the freestream flow past the wing, at various vertical and spanwise locations. The nondimensional loading along the wing span is taken to be

$$g_e = z^2\sqrt{1 - z^2}$$

with the z axis originating at one tip of the wing so that z = 1 represents the other tip. This type of loading has resemblance to the typical loading on a helicopter rotor blade.

For a particle travelling with constant velocity in the x direction, at constant values of y and z, the nondimensional vertical velocity induced by the wing may be written as

$$v = \frac{1}{4A} \int_{x_1}^{x_2} \left\{ \frac{\partial}{\partial y}\, y \int_0^1 \frac{\zeta^2\sqrt{1 - \zeta^2}\, d\zeta}{\left[x^2 + y^2 + (z - \zeta)^2\right]^{3/2}} \right\} dx$$

$$4Av = \int_{x_1}^{x_2} dx \int_0^1 \zeta^2\sqrt{1 - \zeta^2}\, d\zeta \left[\frac{1}{\left[x^2 + y^2 + (z - \zeta)^2\right]^{3/2}} - \frac{3y^2}{\left[x^2 + y^2 + (z - \zeta)^2\right]^{5/2}} \right]$$

$$4Av = \int_0^1 \zeta^2 \sqrt{1-\zeta^2}\, d\zeta \left[\frac{x}{(y^2 + (z-\zeta)^2)_d} + \frac{y^2}{xd^3} \right.$$

$$\left. - \frac{y^2 d}{\left[y^2 + (z-\zeta)^2\right]^2 x} - \frac{y^2 x}{\left[y^2 + (z-\zeta)^2\right]^2 d} \right] \Bigg|_{x=x_1}^{x=x_2} \qquad \text{(D 3)}$$

where $d = \left[x^2 + y^2 (z-\zeta)^2\right]^{1/2}$

The integral with respect to ζ can be numerically evaluated. The induced velocity can also be calculated with a piecewise constant or piecewise quadratic approximation to g, using integrals similar to those listed in Appendix B, but the details of these expressions will not be written out here. For the calculation, $x_1 = -1$ and $x_2 = 1$, while the spanwise division for the approximations was done with 2 models: (1) three segments along the span, with $\Delta\zeta_j = 0.5, 0.3, 0.2$; and, (2) five segments along the span, with $\Delta\zeta_j = 0.5, 0.2, 0.1, 0.1, 0.1$. The results of the calculations are shown in tables D 2 and D 3 where the abbreviations p.c. and p.q. represent the piecewise constant and piecewise quadratic schemes. These induced velocity comparisons are also plotted in figure 4.

TABLE D 2. INDUCED VELOCITY COMPARISON FOR THREE-SEGMENT SPANWISE APPROXIMATIONS

Vertical distance, y	Spanwise location, z = 0.25			Spanwise location, z = 0.65			Spanwise location, z = 0.9		
	Exact	p.c.	p.q.	Exact	p.c.	p.q.	Exact	p.c.	p.q.
0.01	1.144	-0.603	-1.071	5.147	5.426	4.772	11.454	9.247	12.468
0.02	-1.050	-0.596	-0.987	5.037	5.381	4.735	10.455	9.024	11.017
0.05	-0.791	-0.548	-0.755	4.693	5.094	4.565	7.831	7.762	7.773
0.10	-0.440	-0.401	-0.430	4.099	4.343	4.128	5.007	5.391	4.849
0.20	0.026	-0.042	0.018	3.012	2.963	3.086	2.692	2.881	2.644
0.40	0.375	0.334	0.369	1.605	1.522	1.625	1.311	1.351	1.302
0.60	0.394	0.373	0.392	0.924	0.884	0.927	0.786	0.793	0.781
0.80	0.327	0.316	0.326	0.574	0.555	0.573	0.509	0.508	0.505
1.00	0.253	0.247	0.252	0.377	0.368	0.376	0.344	0.343	0.342

TABLE D 3. INDUCED VELOCITY COMPARISON FOR FIVE-SEGMENT SPANWISE APPROXIMATIONS

Vertical distance, y	Spanwise location, z = 0.25			Spanwise location, z = 0.60			Spanwise location, z = 0.95		
	Exact	p.c.	p.q.	Exact	p.c.	p.q.	Exact	p.c.	p.q.
0.01	-1.144	-0.518	-1.101	4.037	5.206	4.125	11.708	9.139	12.651
0.02	-1.050	-0.512	-1.013	3.975	5.120	4.048	9.481	8.404	9.495
0.05	-0.791	-0.470	-0.770	3.771	4.626	3.813	5.274	5.711	5.057
0.10	-0.440	-0.341	-0.432	3.393	3.661	3.406	2.963	3.386	2.876
0.20	0.026	-0.022	0.025	2.629	2.464	2.624	1.845	2.011	1.823
0.40	0.375	0.324	0.372	1.502	1.365	1.496	1.093	1.117	1.085
0.60	0.394	0.363	0.392	0.892	0.824	0.887	0.706	0.700	0.702
0.80	0.327	0.308	0.326	0.562	0.527	0.559	0.474	0.462	0.471
1.00	0.253	0.241	0.252	0.372	0.352	0.370	0.327	0.317	0.325

APPENDIX E

FINAL EQUATIONS AND OUTPUT QUANTITIES

The basic solution is for the spanwise and azimuthwise variation of the dipole strength function, g. With the span divided into J segments, the value at the midpoint of each segment is given the following harmonic representation over the azimuth.

$$\frac{g(r_j)}{\rho \Omega^2 R_1^2} = G_j^o + \sum_{n=1}^{N_h} \left[G_{jn}^c \cos(n\Psi_b) + G_{jn}^s \sin(n\Psi_b) \right] \qquad \text{(E 1)}$$

In the present calculation, the above formula serves only as an interpolation.

The boundary condition to be satisfied states that the normal velocity induced at a point on the blade by the combined pressure field of all the blades is equal to the normal velocity due to blade motion. If w_b denotes the normal velocity due to blade motion, the boundary condition can be symbolically written as

$$\frac{w_b}{\Omega R_1}(r_{bo}, \Psi_{bo}) = \sum_{\substack{\text{no. of} \\ \text{blades}}} \left\{ \sum_i \sum_j (\Delta w_{far})_{ij} \frac{g_i(r_j)}{\rho \Omega^2 R_1^2} \right.$$

$$+ \sum_i (\Delta w_{common})_i \frac{g_i(r_{j'})}{\rho \Omega^2 R_1^2}$$

$$\left. + \sum_i \sum_k \left[(\Delta w_{near}^{I})_{ik} \frac{g_i(r_{j'})}{\rho \Omega^2 R_1^2} + (\Delta w_{near}^{II})_{ik} \right] \right\} \qquad \text{(E 2)}$$

The contributions Δw can be calculated with either the piecewise constant or piecewise quadratic spanwise representation, as described in Appendix C. The index j' refers to the spanwise segment within which the i^{th} trajectory segment is located (if the i^{th} trajectory segment ranges over more than one spanwise segment, Δw must be summed over these segments as well).

$$\frac{g_i(r_j)}{\rho \Omega^2 R_1^2} = G_j^o + \sum_{n=1}^{N_h} \left[G_{jn}^c \cos(n\Psi_{bi}) + G_{jn}^s \sin(n\Psi_{bi}) \right] \qquad \text{(E 3)}$$

where Ψ_{bi} is any typical point of the i^{th} azimuth interval (e.g., either end or the midpoint). It must be noted that the collective pitch, coning angle and the cyclic pitch coefficients are contained both in w_b and in the near field contribution (Δw_{near}), which is proportional to the functions F_2 and F_3. These are defined below

$$\frac{w_b}{\Omega R_1} = \left[\left\{\theta_o - \epsilon \frac{r_b - R_o}{R_1 - R_o}\right\} \frac{r_b}{R_1} - \mu\alpha_r - \mu \frac{a_1}{2}\right]$$

$$+ \left[b_1 \frac{r_b}{R_1} - \mu a_o\right] \cos\Psi_b + \left[-a_1 \frac{r_b}{R_1} + \mu \left\{\theta_o\right.\right.$$

$$\left.\left. - \epsilon \frac{r_b - R_o}{R_1 - R_o}\right\}\right] \sin\Psi_b + \left[\mu \frac{a_1}{2}\right] \cos 2\Psi_b$$

$$+ \left[\mu \frac{b_1}{2}\right] \sin 2\Psi_b \qquad \text{(E 4)}$$

$$\left.\begin{aligned} F_2 &= \left[2\mu\theta_o + 2\mu\epsilon \frac{R_o}{R_1 - R_o}\right] \cos\Psi_b + \left[2\mu a_o\right] \sin\Psi_b \\ &+ \left[2\mu b_1\right] \cos 2\Psi_b + \left[-2\mu a_1 - \mu^2 \epsilon \frac{R_1}{R_1 - R_o}\right] \sin 2\Psi_b \\ F_3 &= a_o + \left[-2a_1 - 4\mu\epsilon \frac{R_1}{R_1 - R_o}\right] \cos\Psi_b + \left[-2b_1\right] \sin\Psi_b \end{aligned}\right\} \qquad \text{(E 5)}$$

For presentation as output, the following quantities are calculated:

(1) azimuthwise variations of total lift per blade, aerodynamic moment about the hub and spanwise center of lift location,

(2) spanwise and azimuthwise variations of sectional lift, pitching moment about quarter-chord and center of pressure location,

(3) chordwise, spanwise and azimuthwise variations of surface pressure differential. The expressions for these quantities are presented below.

Surface pressure differential,

$$\frac{\Delta p}{\rho \Omega^2 R_1^2} = 2\left[- \frac{g}{\rho \Omega^2 R_1^2} \sqrt{\frac{1-x}{1+x}} + \frac{(1-\xi)}{2A} (F_2 + \frac{r_b}{R_1} F_3) \sqrt{1-x^2} \right] \quad \text{(E 6)}$$

where x is nondimensional with respect to the semi-chord.

Sectional lift,

$$\frac{\ell}{\rho \Omega^2 R_1^3} = - \frac{\pi}{A} (1-\xi) \left[\frac{g}{\rho \Omega^2 R_1^2} - \frac{(1-\xi)}{4A} (F_2 + \frac{r_b}{R_1} F_3) \right] \quad \text{(E 7)}$$

Pitching moment about quarter-chord,

$$\frac{m}{\rho \Omega^2 R_1^4} = - \frac{\pi}{16 A^3} (1-\xi)^3 (F_2 + \frac{r_b}{R_1} F_3) \quad \text{(E 8)}$$

Center of pressure location (from leading edge), as a fraction of the chord,

$$\frac{x_{cp}}{c} = 0.25 + \frac{A}{(1-\xi)} \frac{m}{R_1 \ell} \quad \text{(E 9)}$$

Total lift per blade,

$$\begin{aligned} \frac{L}{\rho \Omega^2 R_1^4} = & - \frac{\pi}{A} (1-\xi) \int_{\xi}^{1} \frac{g}{\rho \Omega^2 R_1^2} d\left(\frac{r_b}{R_1}\right) \\ & + \frac{\pi (1-\xi)^2}{4A^2} \left\{ \frac{(1-\xi^2)}{2} a_o + \left[2\mu\theta_o (1-\xi) - a_1 (1-\xi^2) - 2\mu\epsilon \right] \cos \Psi_b \right. \\ & + \left[2\mu a_o (1-\xi) - b_1 (1-\xi^2) \right] \sin \Psi_b + \left[2\mu b_1 (1-\xi) \right] \cos 2\Psi_b \\ & \left. + \left[- 2\mu a_1 (1-\xi) - \mu^2 \epsilon \right] \sin 2\Psi_b \right\} \end{aligned} \quad \text{(E 10)}$$

Aerodynamic moment about hub,

$$\frac{M}{\rho \Omega^2 R_1^5} = -\frac{\pi}{A}(1-\xi)\int_{\xi}^{1} \frac{g}{\rho \Omega^2 R_1^2}\frac{r_b}{R_1}\, d\left(\frac{r_b}{R_1}\right)$$

$$+ \frac{\pi(1-\xi)^2}{A^2}\left\{\frac{(1-\xi^3)}{3}a_o + \left[\mu\theta_o(1-\xi^2) - \frac{2a_1}{3}(1-\xi^3)\right.\right.$$

$$\left. + \frac{\mu\epsilon}{3}(-4-\xi-\xi^2)\right]\cos\psi_b$$

$$+ \left[\mu a_o(1-\xi^2) - \frac{2b_1}{3}(1-\xi^3)\right]\sin\psi_b + \left[\mu b_1(1-\xi^2)\right]\cos 2\psi_b$$

$$\left. + \left[-\mu a_1(1-\xi^2) - \frac{\mu^2\epsilon}{2}(1+\xi)\right]\sin 2\psi_b\right\} \qquad \text{(E 11)}$$

Spanwise center of lift location,

$$\frac{r_L}{R_1} = \frac{M}{R_1 L} \qquad \text{(E 12)}$$

The spanwise integrals of g, required in some of the expressions above, are given in Appendix A.

If the collective pitch, coning angle and cyclic pitch coefficients are considered unknown, additional equations are necessary. These equations are given below.

Piecewise Constant Representation

$$-\sum_{j=1}^{J} G_j^o \Delta s_j + \left[\frac{1}{8A}(1-\xi)(1-\xi^2)\right]a_o = \frac{A}{(1-\xi)}\frac{C_T}{B}$$

$$- \sum_{j=1}^{J} G_j^o \, r_j \Delta s_j + \left[\frac{1}{12A} (1 - \xi)(1 - \xi^3) - \frac{2}{\gamma} \right] a_o = 0$$

$$- \sum_{j=1}^{J} G_{j1}^c \, r_j \Delta s_j + \left[\frac{\mu}{4A} (1 - \xi)(1 - \xi^2) \right] \theta_o - \left[\frac{1}{6A} (1 - \xi)(1 - \xi^3) \right] a_1$$

$$= - \frac{\epsilon}{12A} \mu (-4 + 3\xi + \xi^3)$$

$$- \sum_{j=1}^{J} G_{j1}^s \, r_j \Delta s_j + \left[\frac{\mu}{4A} (1 - \xi)(1 - \xi^2) \right] a_o - \left[\frac{1}{6A} (1 - \xi)(1 - \xi^3) \right] b_1 = 0$$

Piecewise Quadratic Representation

In this case, the equations will also involve the values of g at the ends of spanwise segments; however, these can be related to the central values, as described in Appendix A. Let this relation be written symbolically as,

$$\frac{g(s_i)}{\rho \Omega^2 R_1^2} = \sum_{j=1}^{J} h_{ij} \frac{g(r_j)/\rho \Omega^2 R_1^2}{\Delta s_j}$$

Then the equations are as follows.

$$- \sum_{i=1}^{J} \left[4G_i^o + \sum_{j=1}^{J} (h_{ij} + h_{i+1,j}) \frac{G_j^o}{\Delta s_j} \right] \frac{\Delta s_i}{6}$$

$$+ \left[\frac{1}{8A} (1 - \xi)(1 - \xi^2) \right] a_o = \frac{A}{(1 - \xi)} \frac{C_T}{B}$$

$$- \sum_{i=1}^{J} \left[4r_i \, G_i^o + \sum_{j=1}^{J} (s_i \, h_{ij} + s_{i+1} \, h_{i+1,j}) \frac{G_j^o}{\Delta s_j} \right] \frac{\Delta s_i}{6}$$

$$+ \left[\frac{1}{12A} (1 - \xi)(1 - \xi^3) - \frac{2}{\gamma} \right] a_o = 0$$

$$- \sum_{i=1}^{J} \left[4r_i G_{i1}^{c} + \sum_{j=1}^{J} (s_i h_{ij} + s_{i+1} h_{i+1,j}) \frac{G_{j1}^{c}}{\Delta s_j} \right] \frac{\Delta s_i}{6}$$

$$+ \left[\frac{\mu}{4A} (1 - \xi)(1 - \xi^2) \right] \theta_o - \left[\frac{1}{6A} (1 - \xi)(1 - \xi^3) \right] a_1$$

$$= - \frac{\epsilon}{12A} \mu (-4 + 3\xi + \xi^3)$$

$$- \sum_{i=1}^{J} \left[4r_i G_{i1}^{s} + \sum_{j=1}^{J} (s_i h_{ij} + s_{i+1} h_{i+1,j}) \frac{G_{j1}^{s}}{\Delta s_j} \right] \frac{\Delta s_i}{6}$$

$$+ \left[\frac{\mu}{4A} (1 - \xi)(1 - \xi^2) \right] a_o - \left[\frac{1}{6A} (1 - \xi)(1 - \xi^3) \right] b_1 = 0$$

REFERENCES

1. Van Holten, Th.: The Computation of Aerodynamic Loads on Helicopter Blades in Forward Flight, Using the Method of the Acceleration Potential. Rep. VTH-189, Technische Hogeschool Delft, Netherlands, March 1975.

2. Van Holten, Th.: Computation of Aerodynamic Loads on Helicopter Rotor Blades in Forward Flight, Using the Method of the Acceleration Potential. Presented at the 9th Congress of the International Congress of the Aeronautical Sciences, ICAS Paper No. 74-54, Haifa, 1974.

3. Van Holten, Th.: On the Validity of Lifting Line Concepts in Rotor Analysis. Vertica, vol. 1, 1977, pp. 239-254.

4. Van Holten, Th.: Some Notes on Unsteady Lifting Line Theory. Journal of Fluid Mechanics, vol. 77, Part 3, 1976, pp. 561-579.

5. Pierce, G. Alvin; and Vaidyanathan, Anand R.: Helicopter Rotor Loads Using a Matched Asymptotic Expansion Technique. NASA CR-165742, May 1981.

6. Rabbott, J. P., Jr; and Churchill, G. B.: Experimental Investigation of the Aerodynamic Loading on a Helicopter Rotor Blade in Forward Flight. NACA RM L56I07, October 1956.

7. Scheiman, J.: A Tabulation of Helicopter Rotor Blade Differential Pressures, Stresses and Motions as Measured in Flight. NASA TM X-952, March 1964.

8. Rabbott, J. P., Jr,; Lizak, A. A.; and Paglino, V. M.: A Presentation of Measured and Calculated Full-Scale Rotor Blade Aerodynamic and Structural Loads. USAAVLABS Tech. Rep. 66-31, July 1966.

9. Gradshteyn, I. S.; and Ryzhik, I. M.: Table of Integrals, Series and Products. Academic Press, 1980.

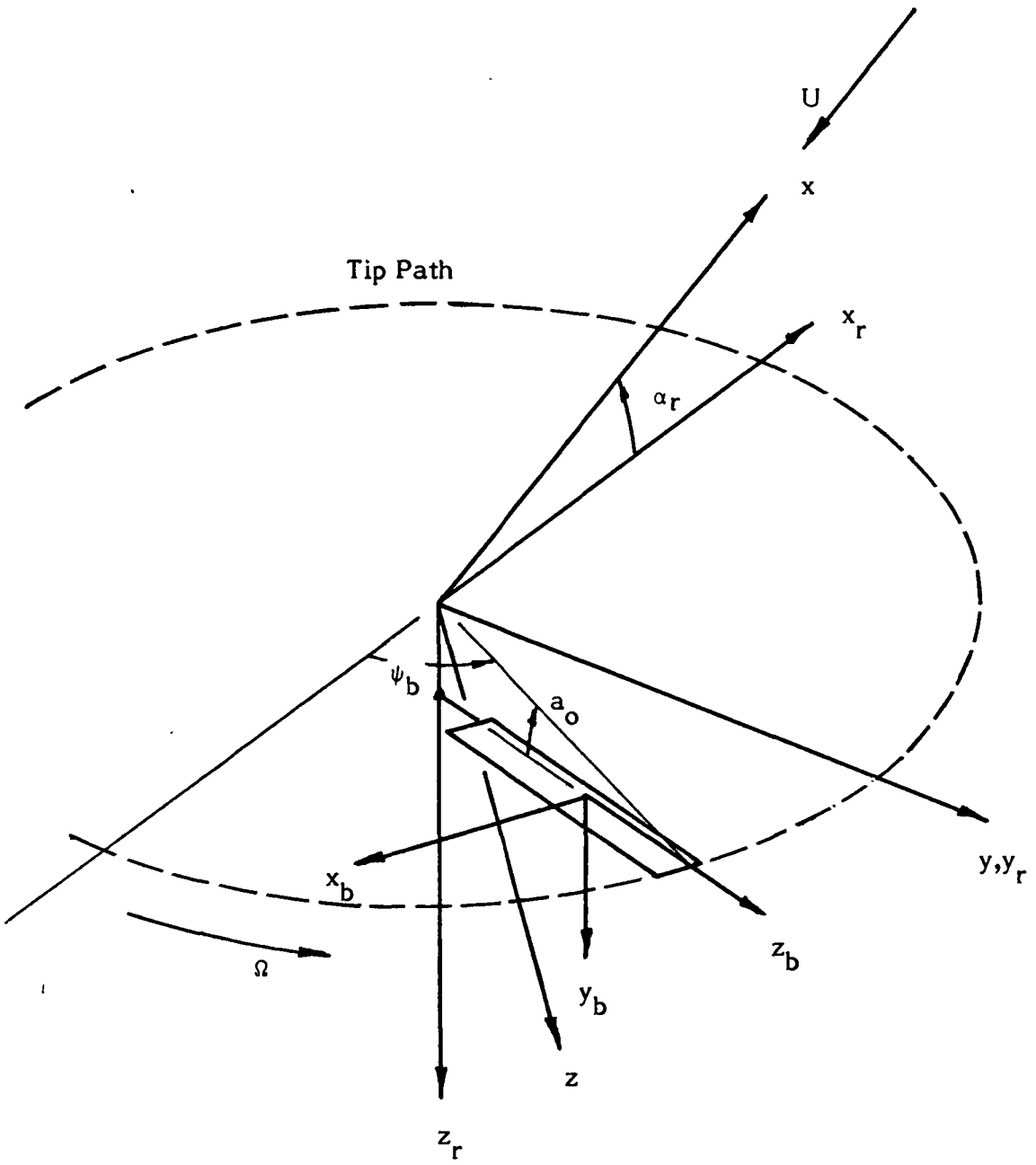

Figure 1. - Rotor coordinate systems.

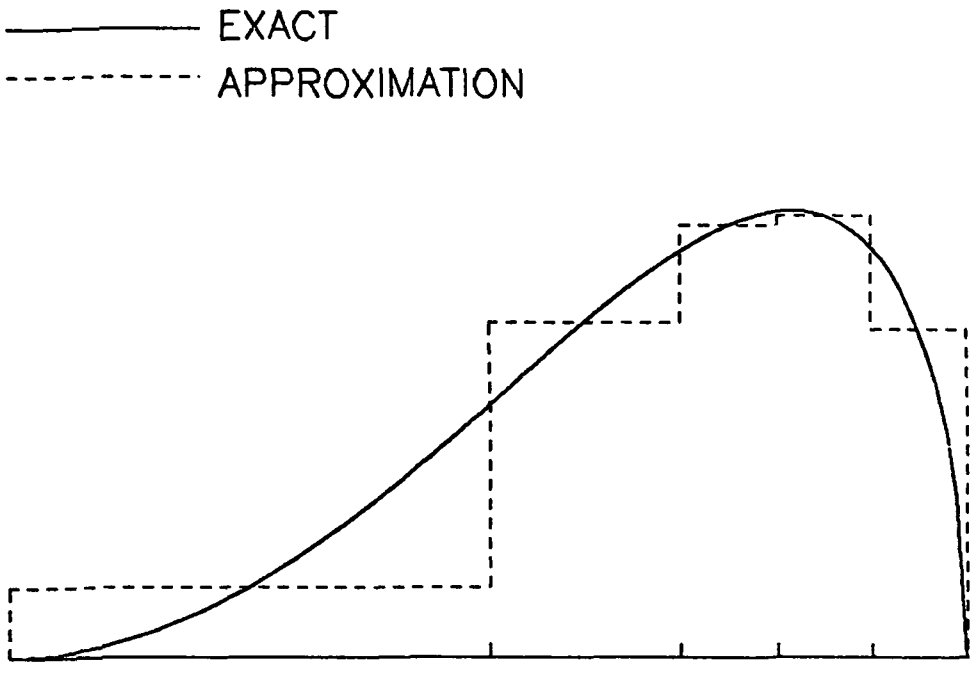

(a) Piecewise constant.

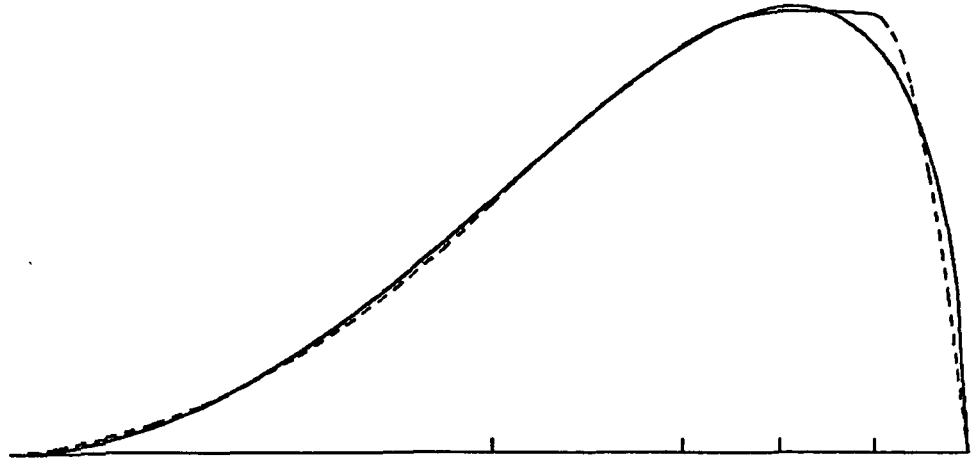

(b) Piecewise quadratic.

Figure 2. - Piecewise continuous representations of the spanwise distribution of doublet strength.

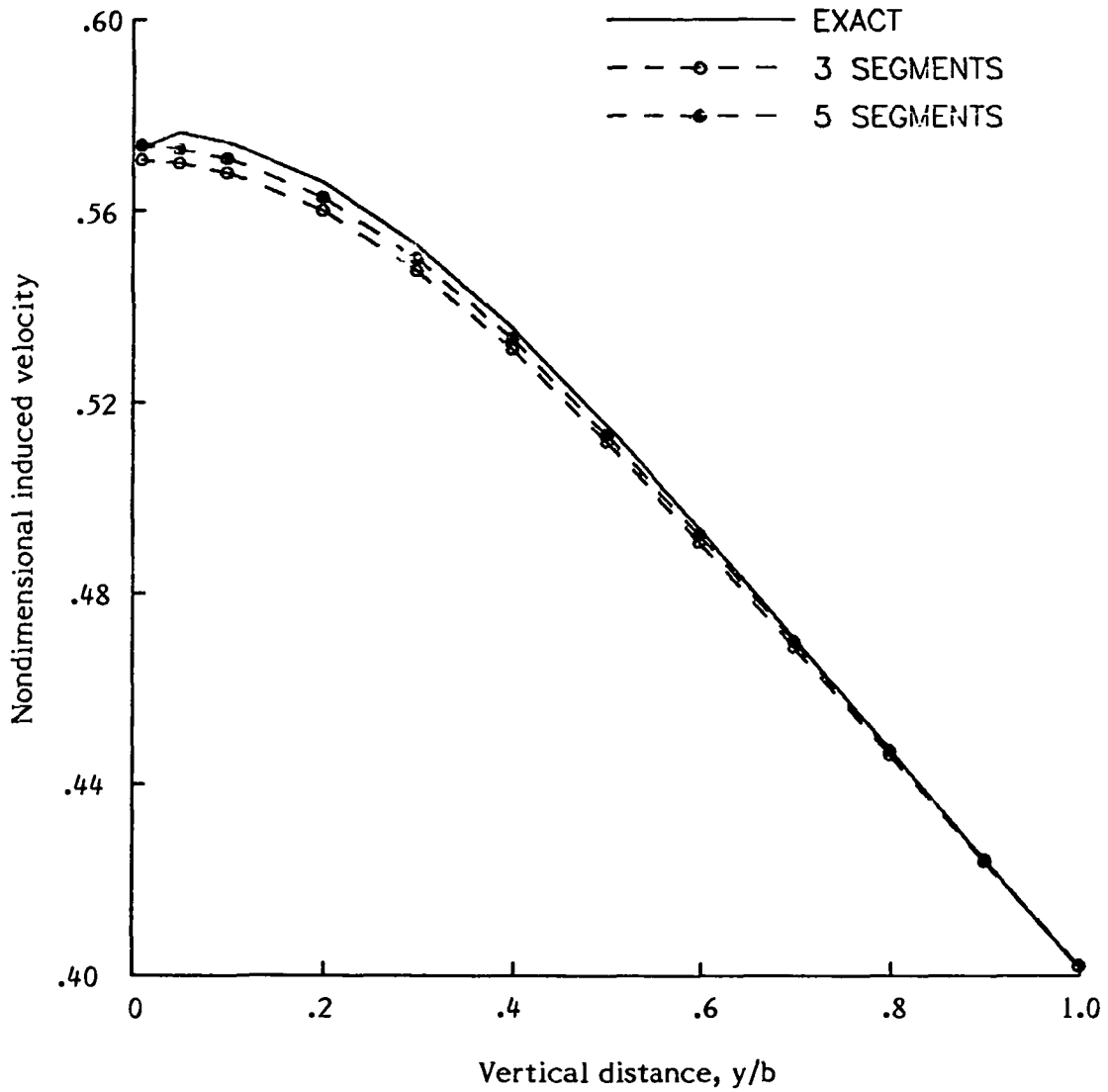

Figure 3. - Induced velocity comparison for piecewise constant chorwise pressure distribution.

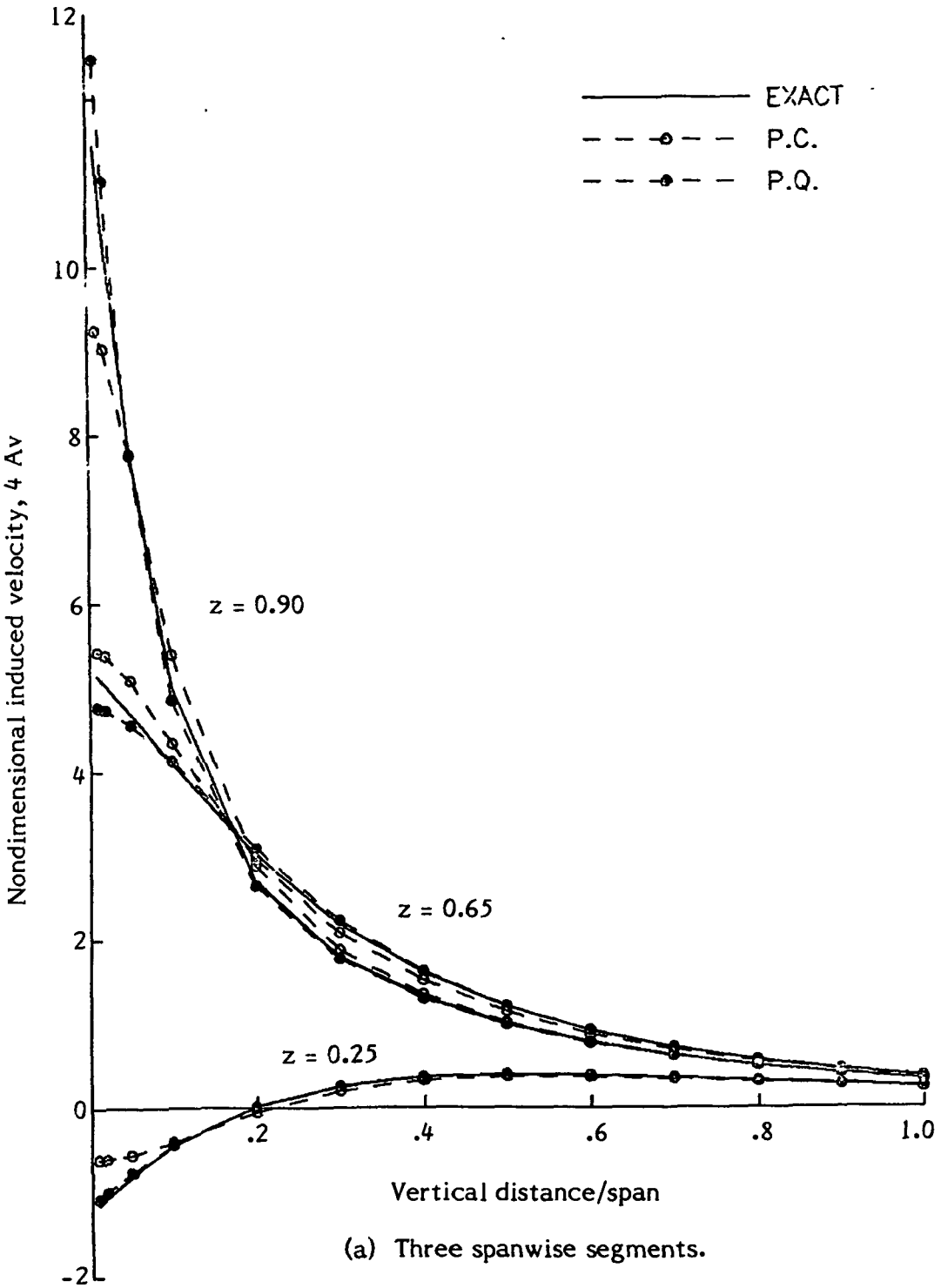

(a) Three spanwise segments.

Figure 4. - Induced velocity comparison for for spanwise approximations.

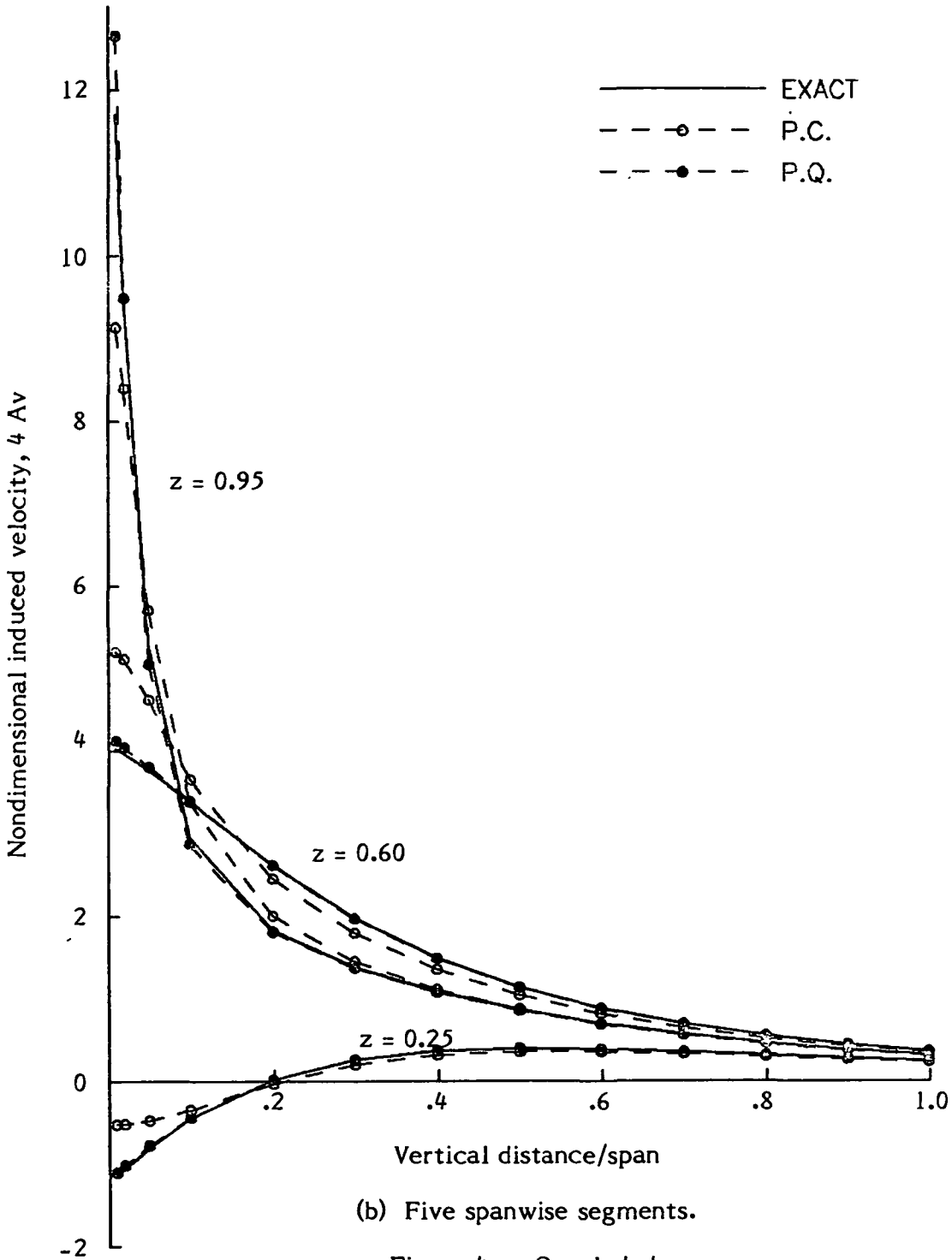

(b) Five spanwise segments.

Figure 4. - Concluded.

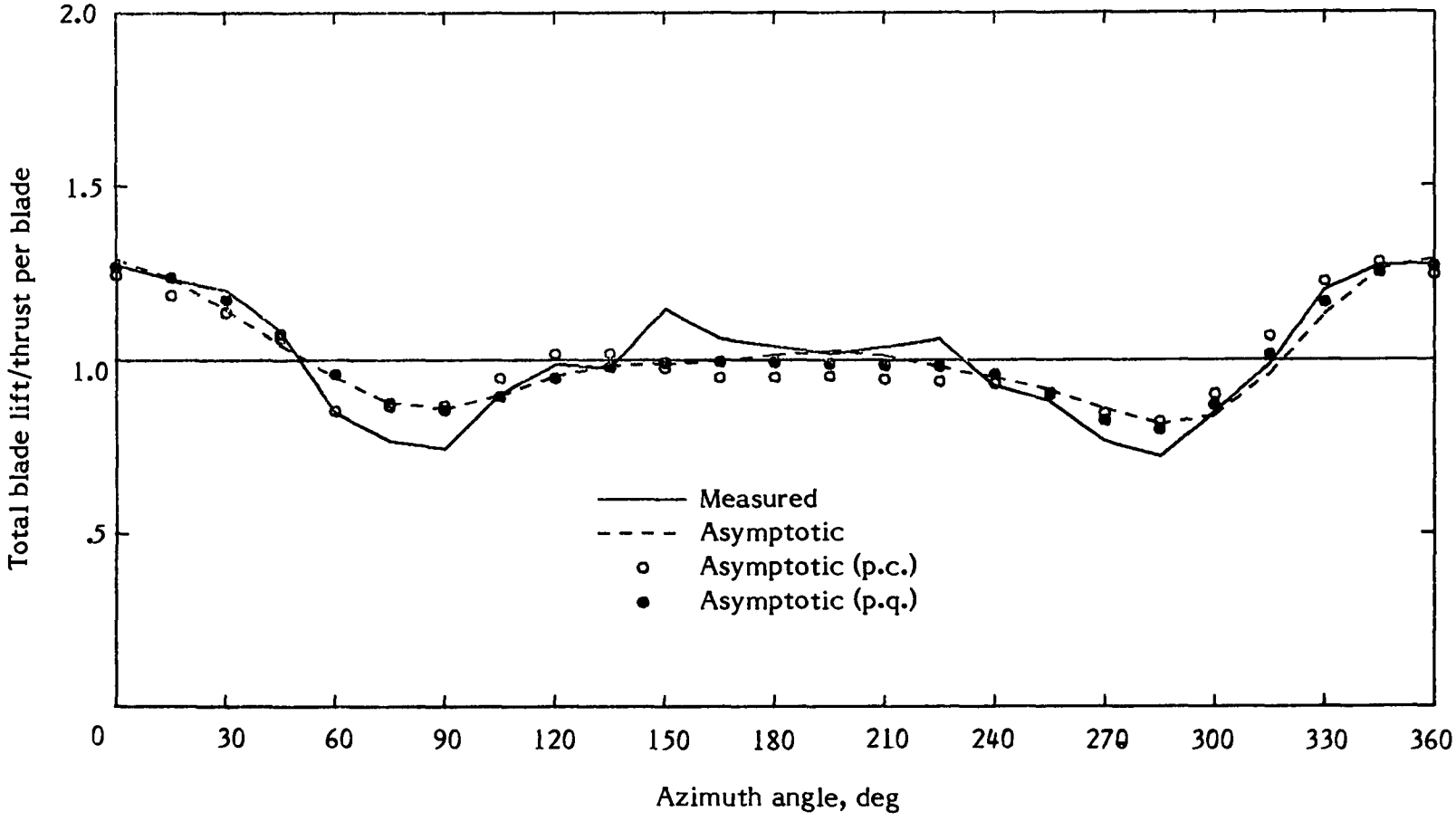

(a) $\mu = 0.08$.

Figure 5. - Total blade lift versus azimuth for Case 1.

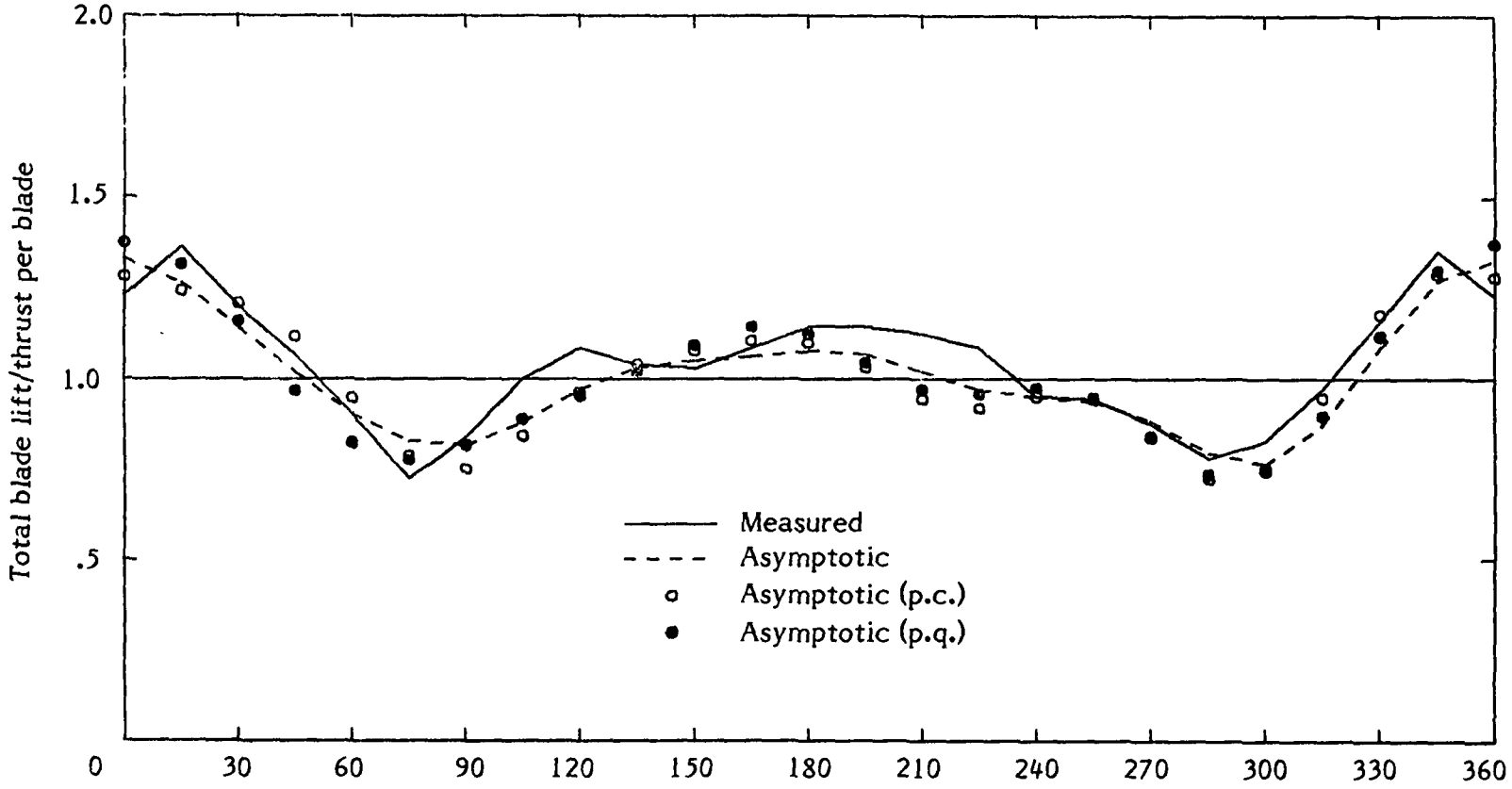

(b) $\mu = 0.15$.

Figure 5. - Continued.

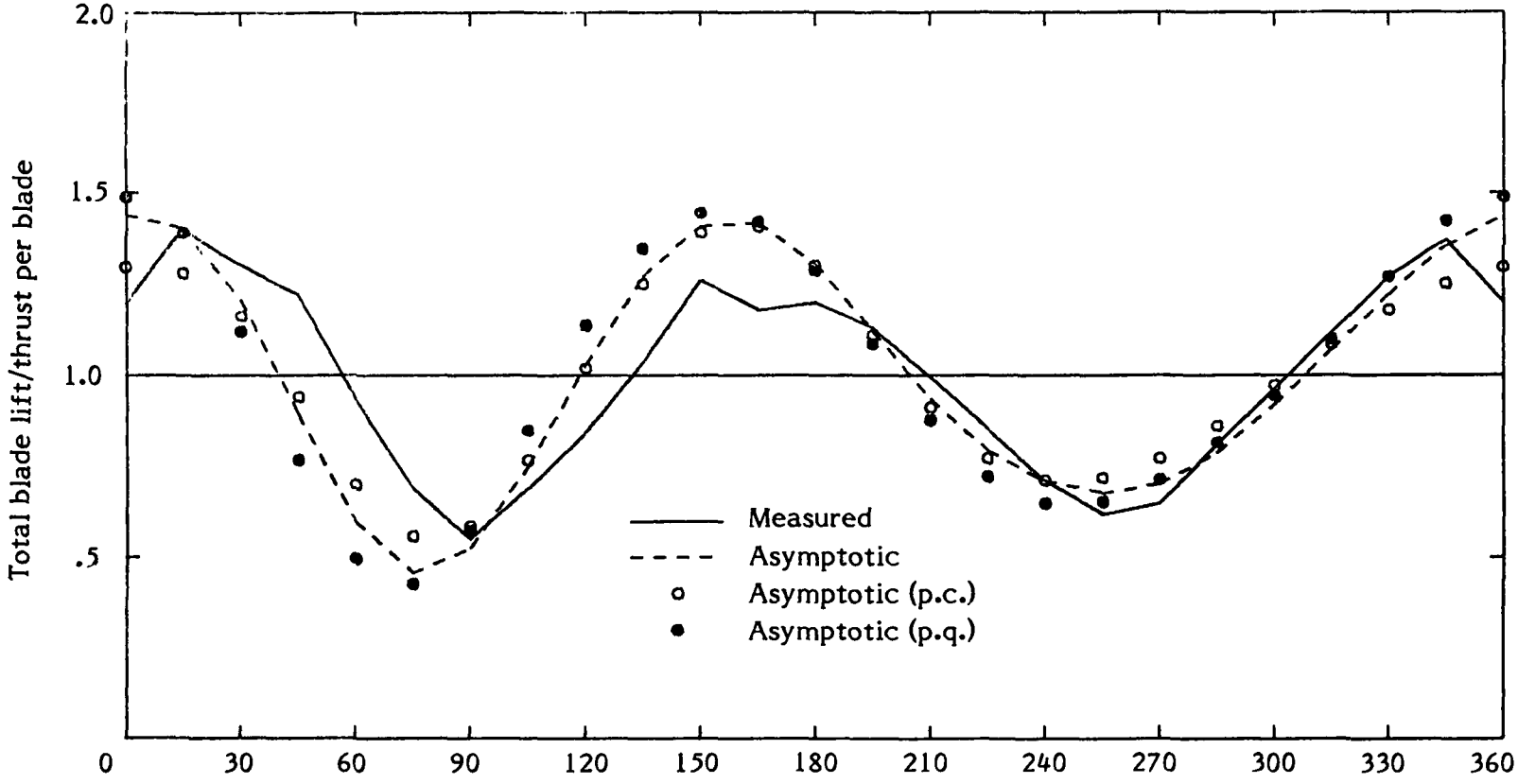

(c) $\mu = 0.29$.

Figure 5. - Concluded.

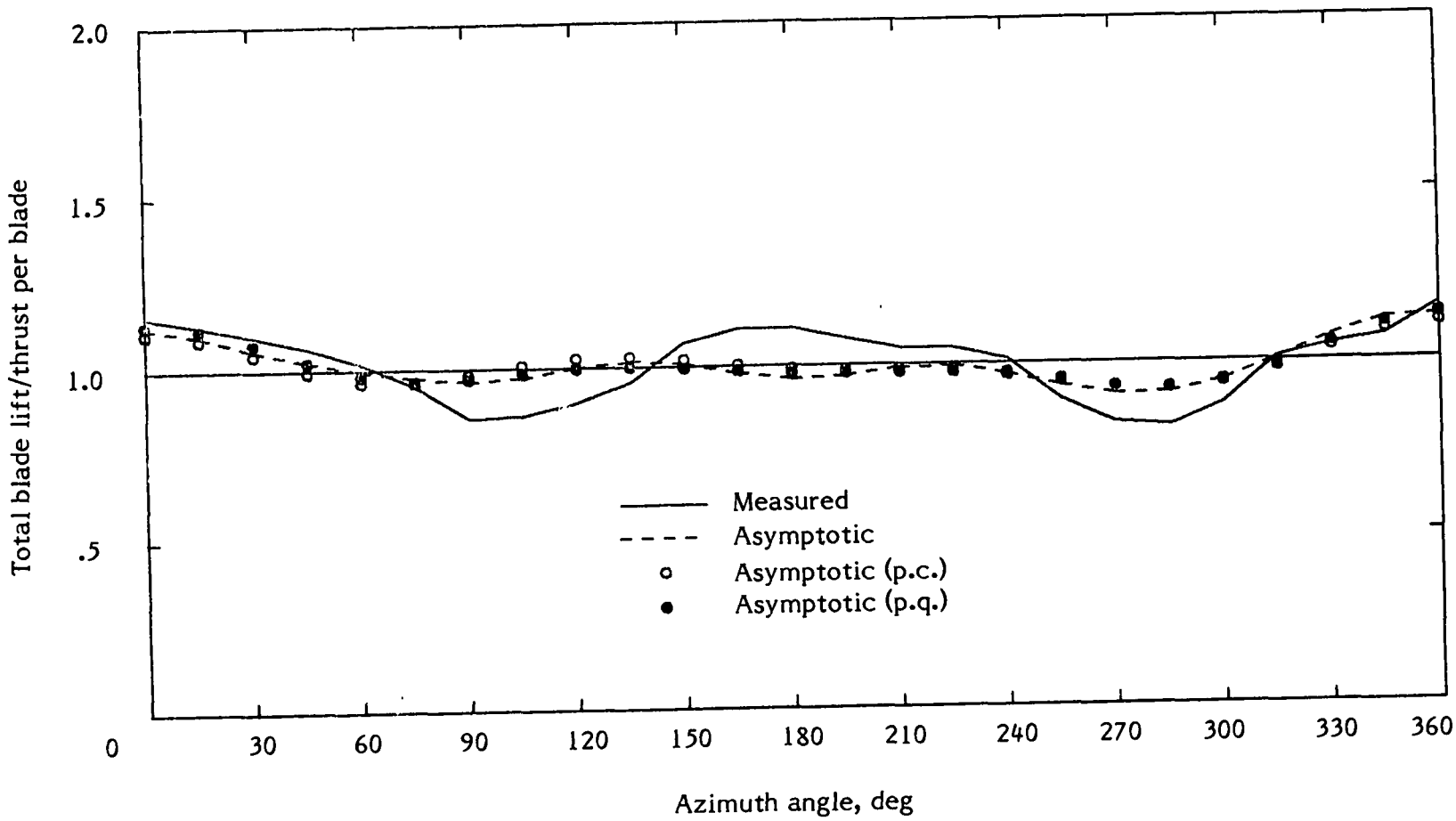

(a) $\mu = 0.06$.

Figure 6. - Total blade lift versus azimuth for Case 2.

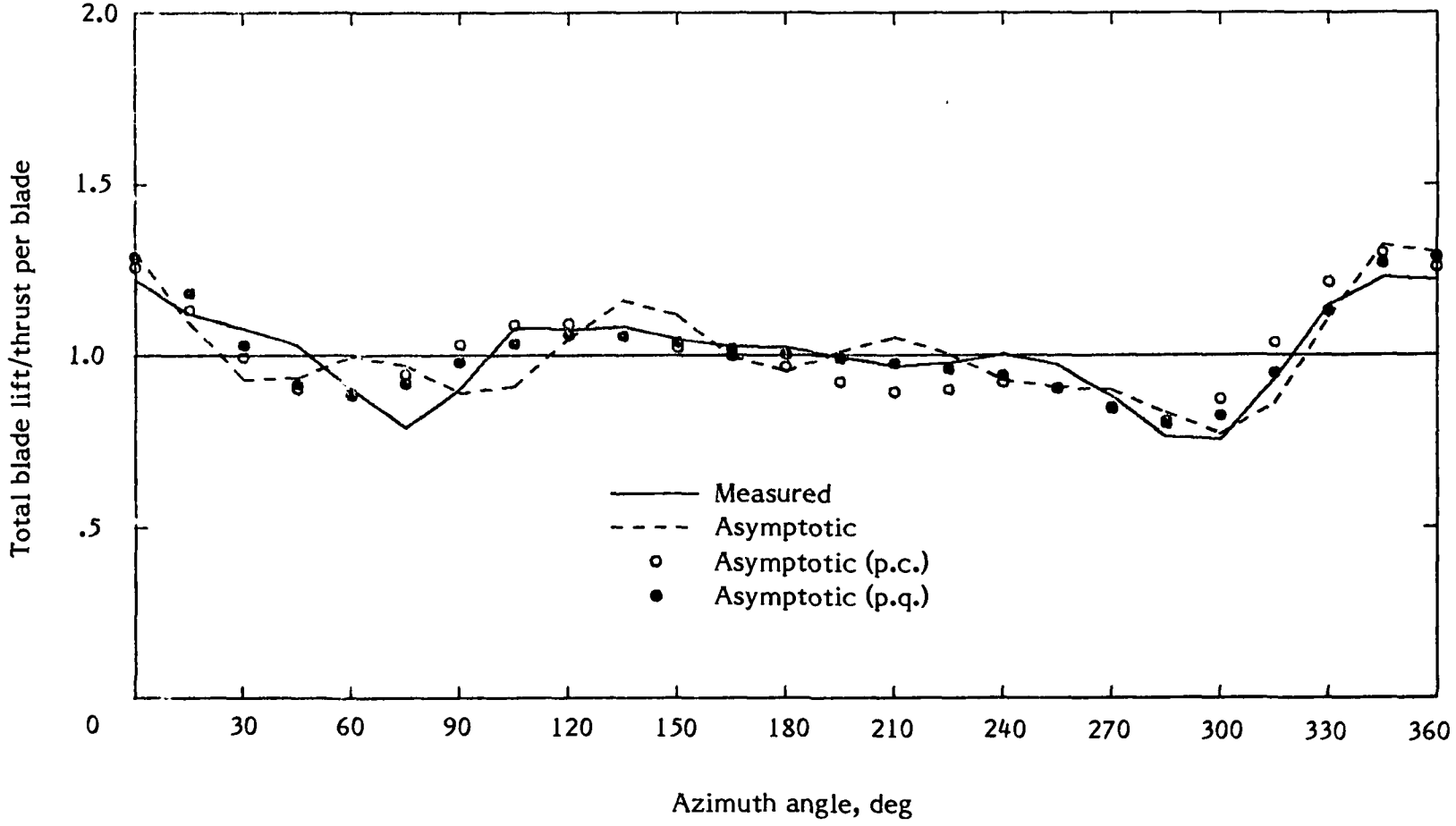

(b) $\mu = 0.13$.

Figure 6. – Continued.

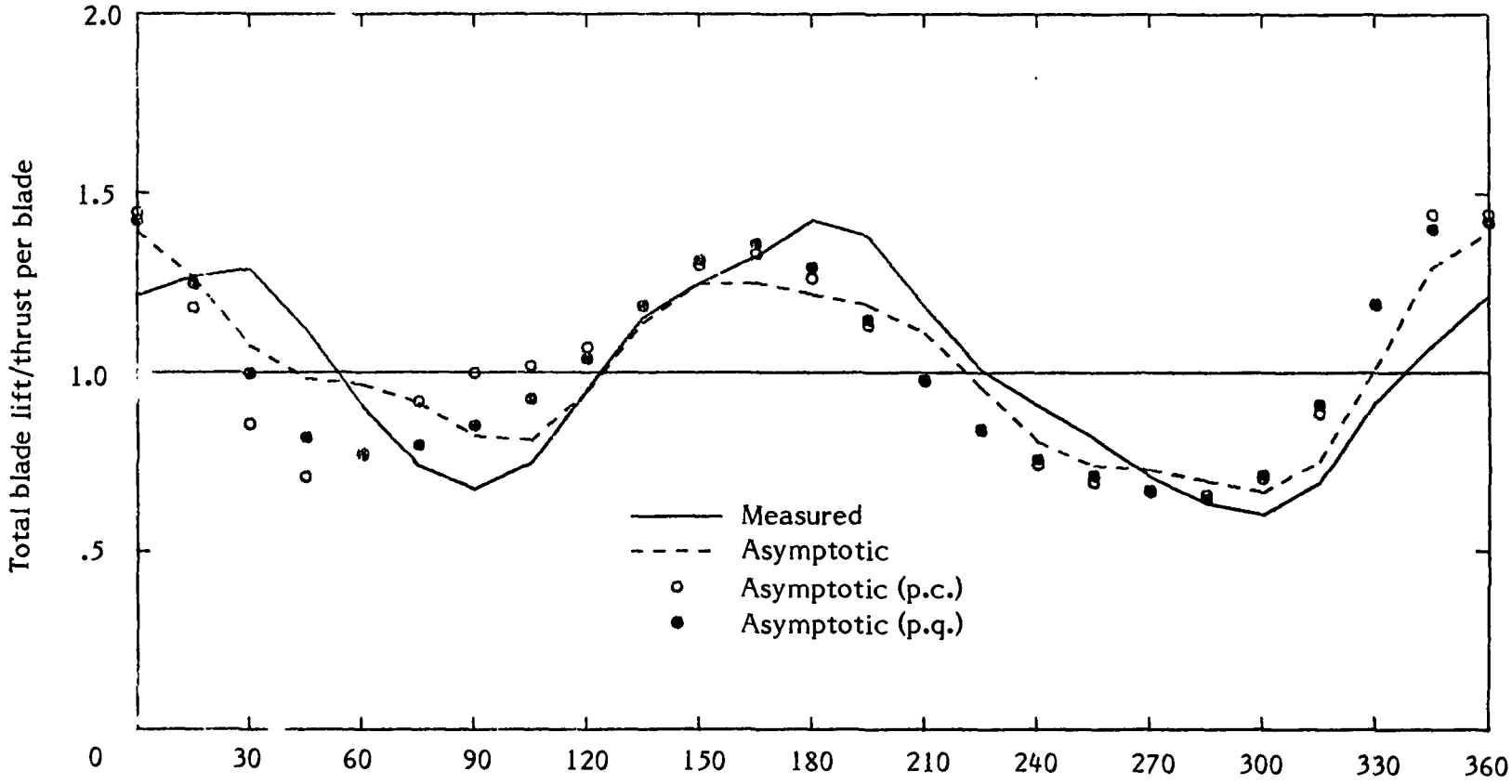

(c) $\mu = 0.29$.

Figure 6. - Concluded.

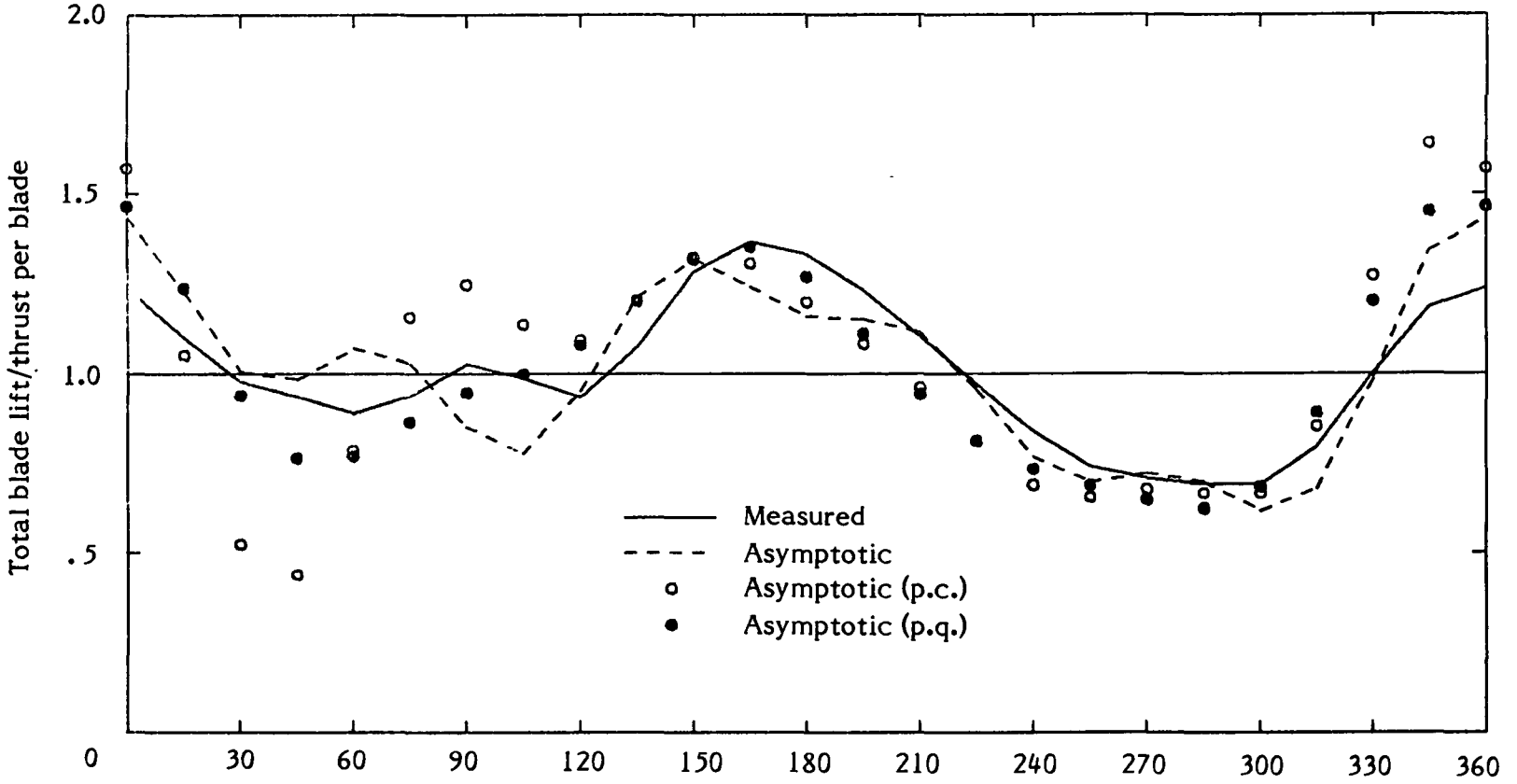

(a) $\mu = 0.29$

Figure 7. - Total blade lift versus azimuth for Case 3.

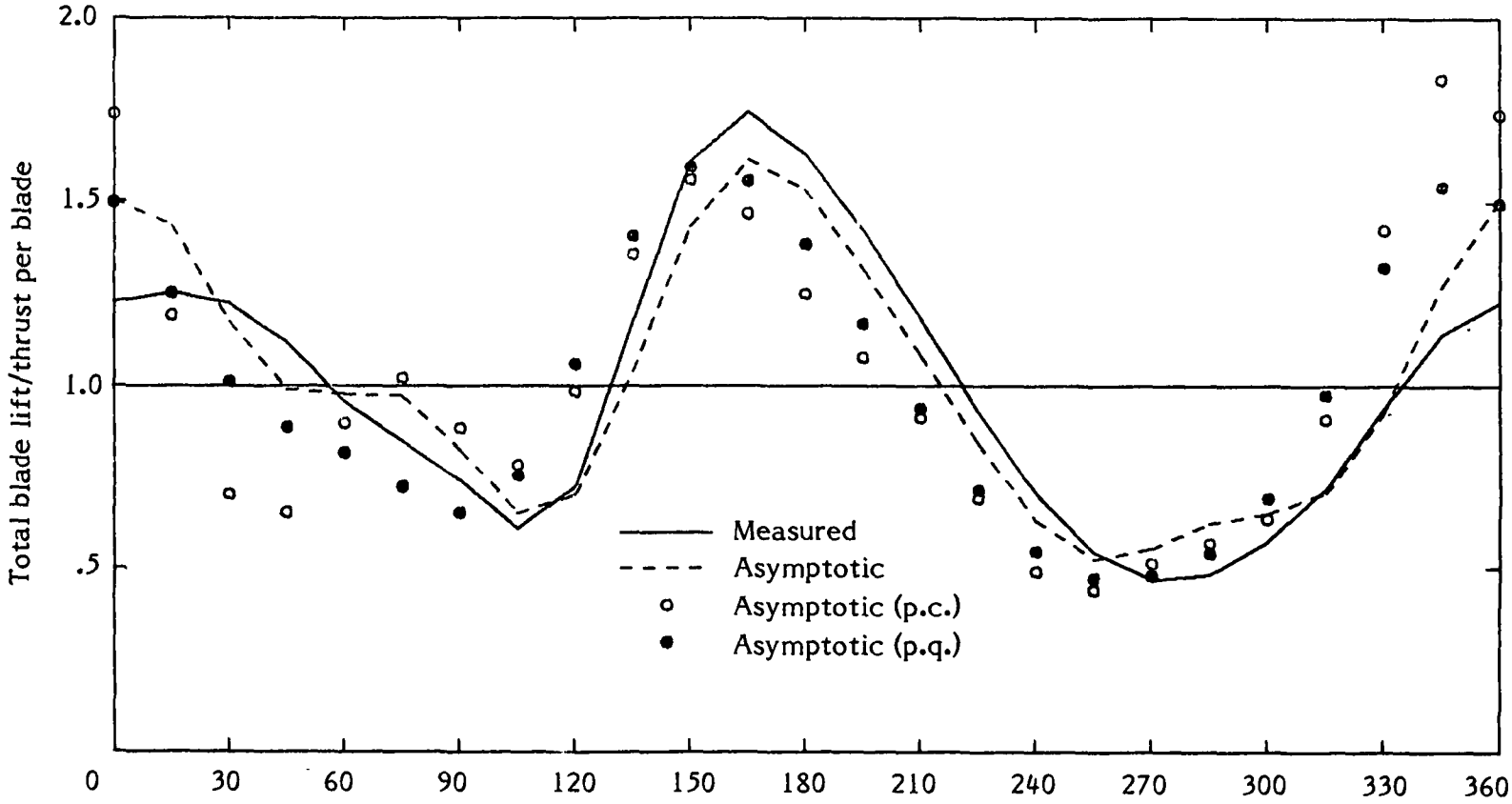

(b) $\mu = 0.39$.

Figure 7. - Continued.

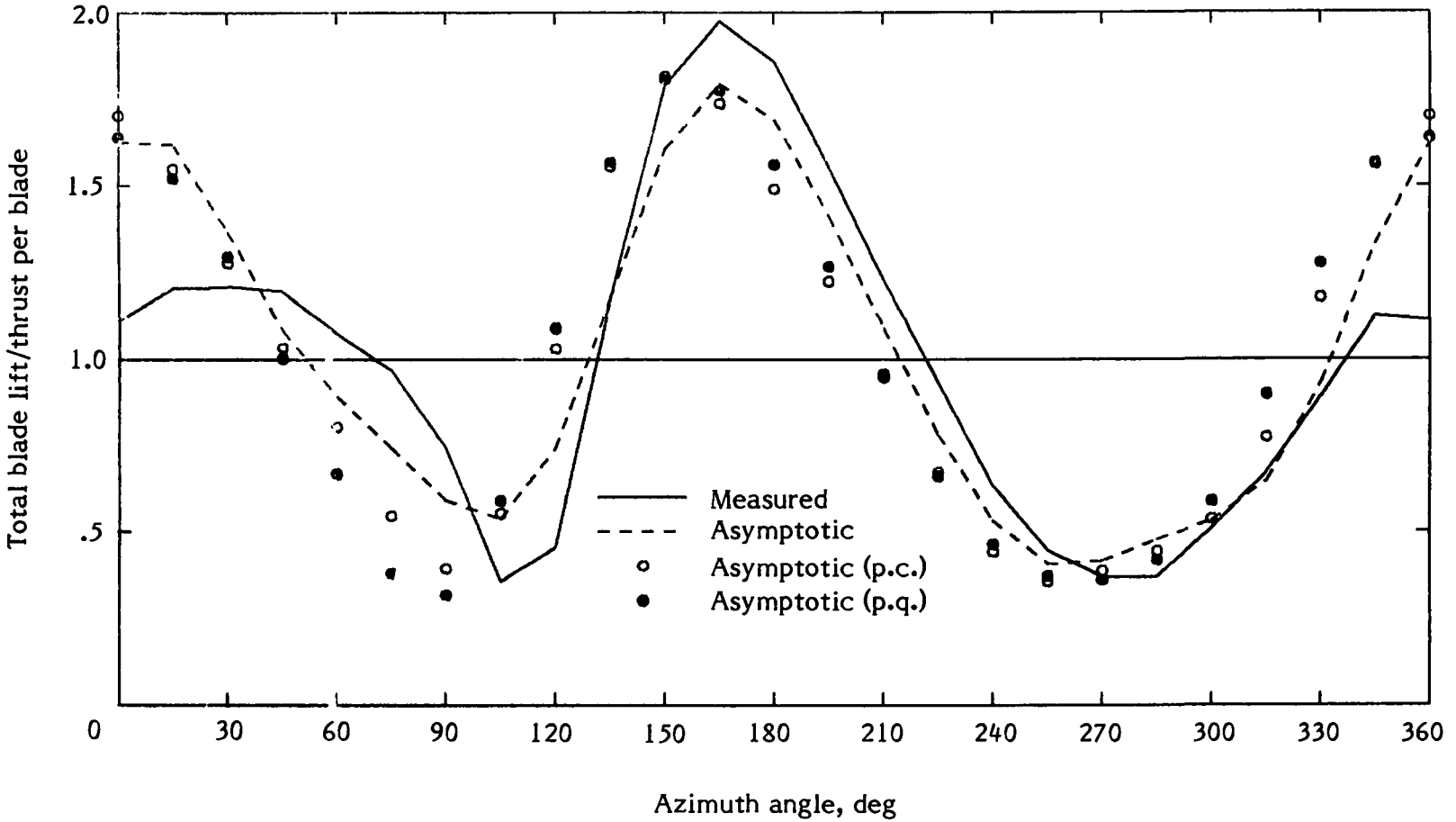

(c) $\mu = 0.45$.

Figure 7. - Concluded.

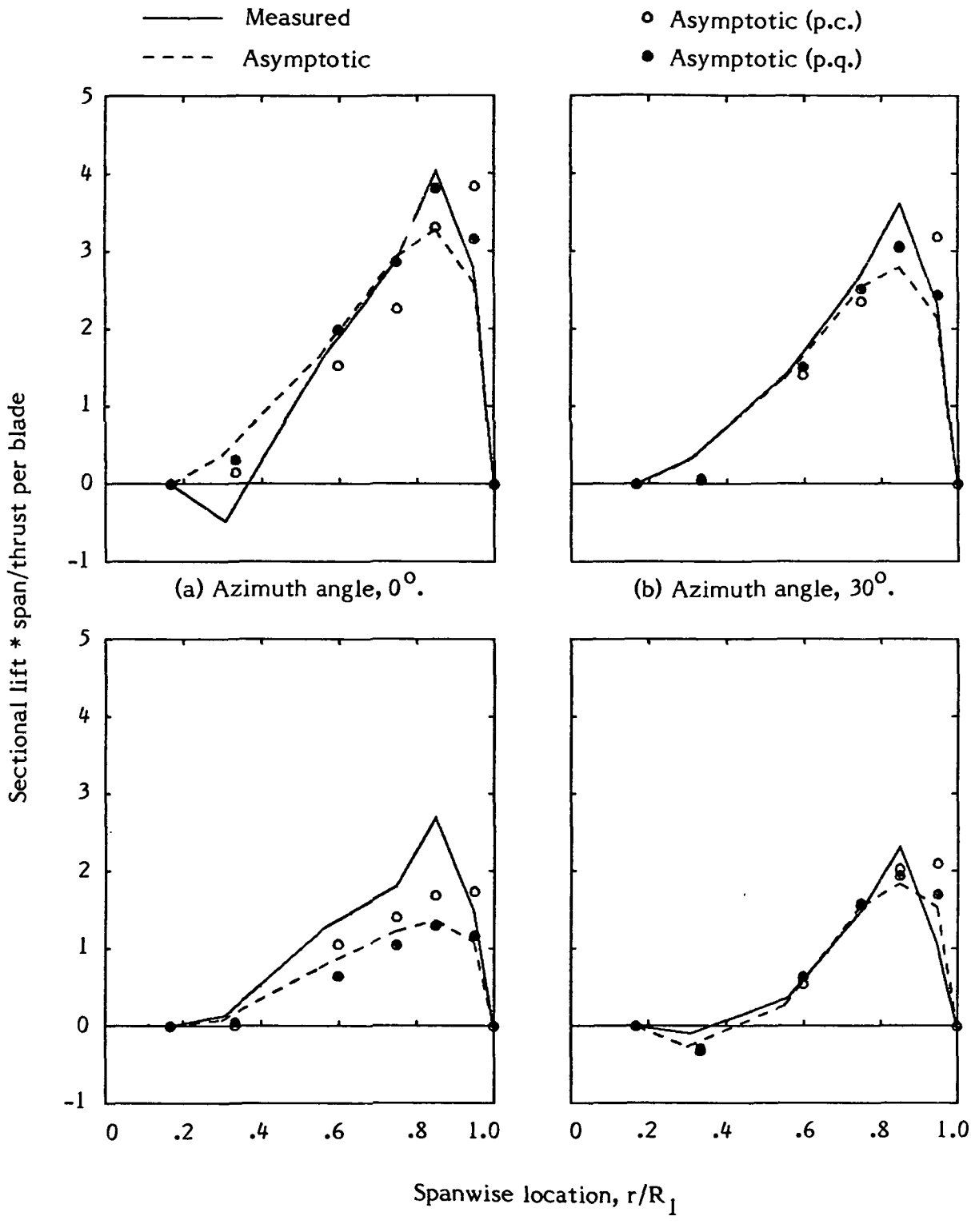

Figure 8. - Sectional lift versus spanwise location for Case 1, $\mu = 0.29$.

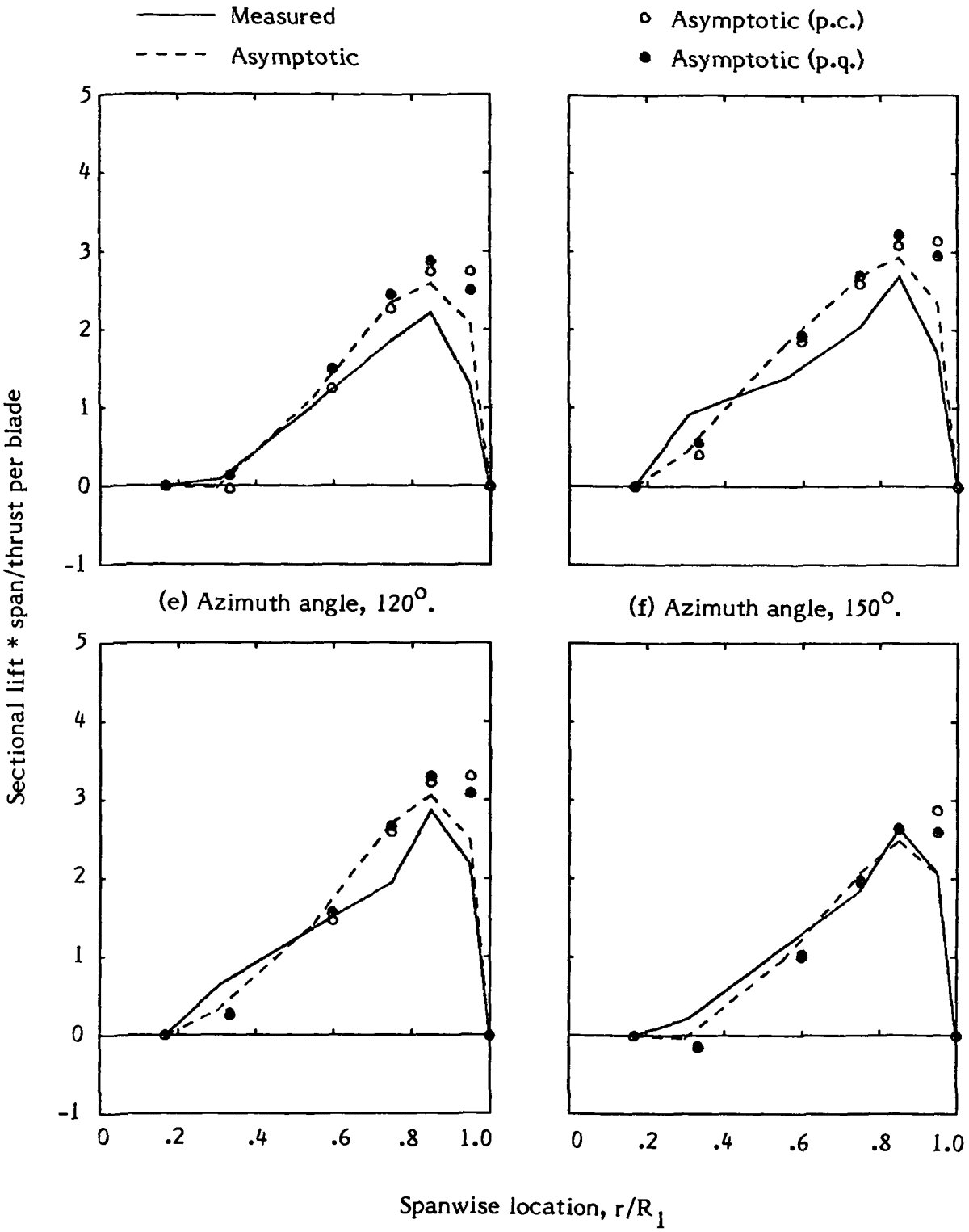

Figure 8. - Continued.

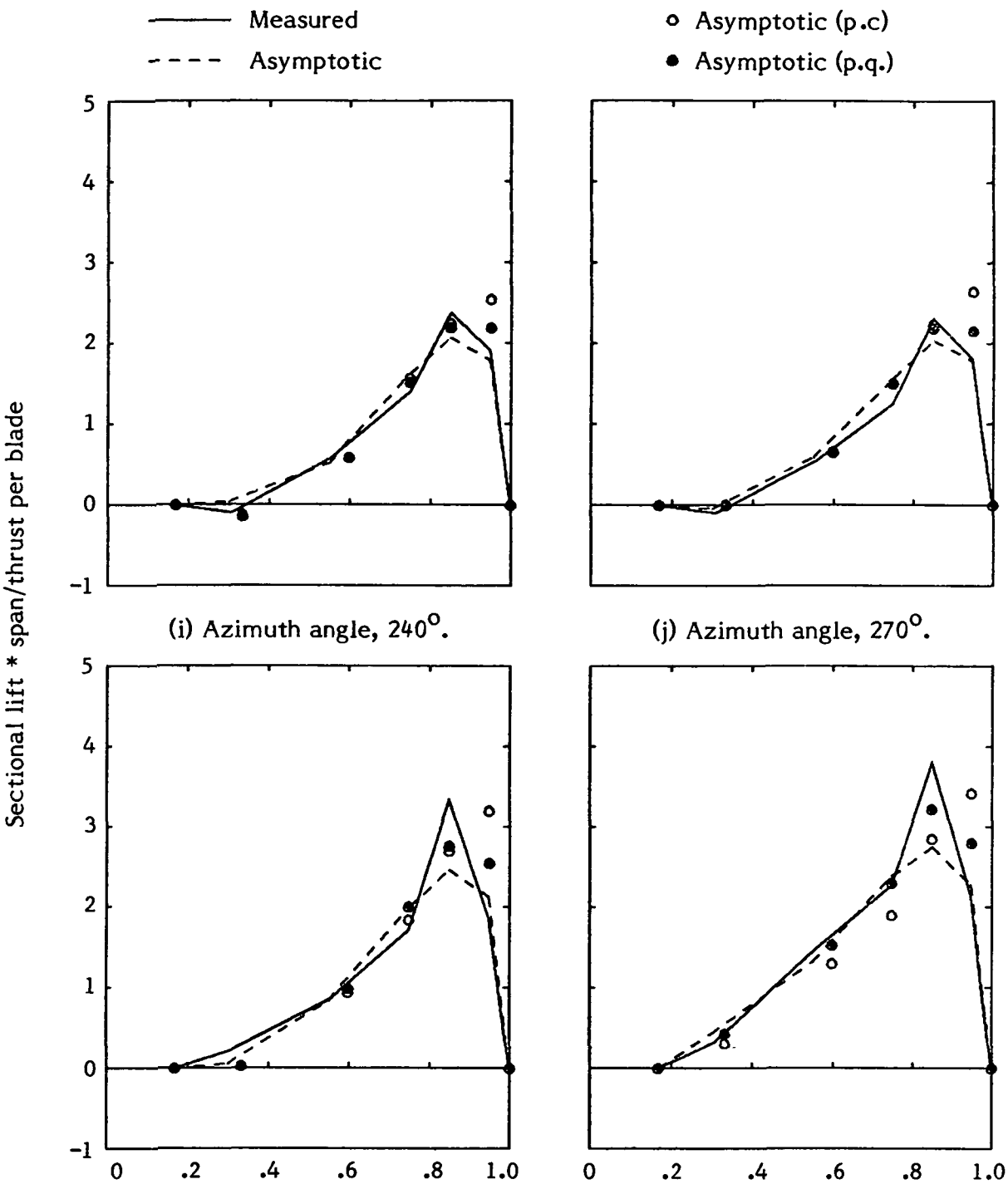

(i) Azimuth angle, 240°.

(j) Azimuth angle, 270°.

(k) Azimuth angle, 300°.

(l) Azimuth angle, 330°.

Figure 8. - Concluded.

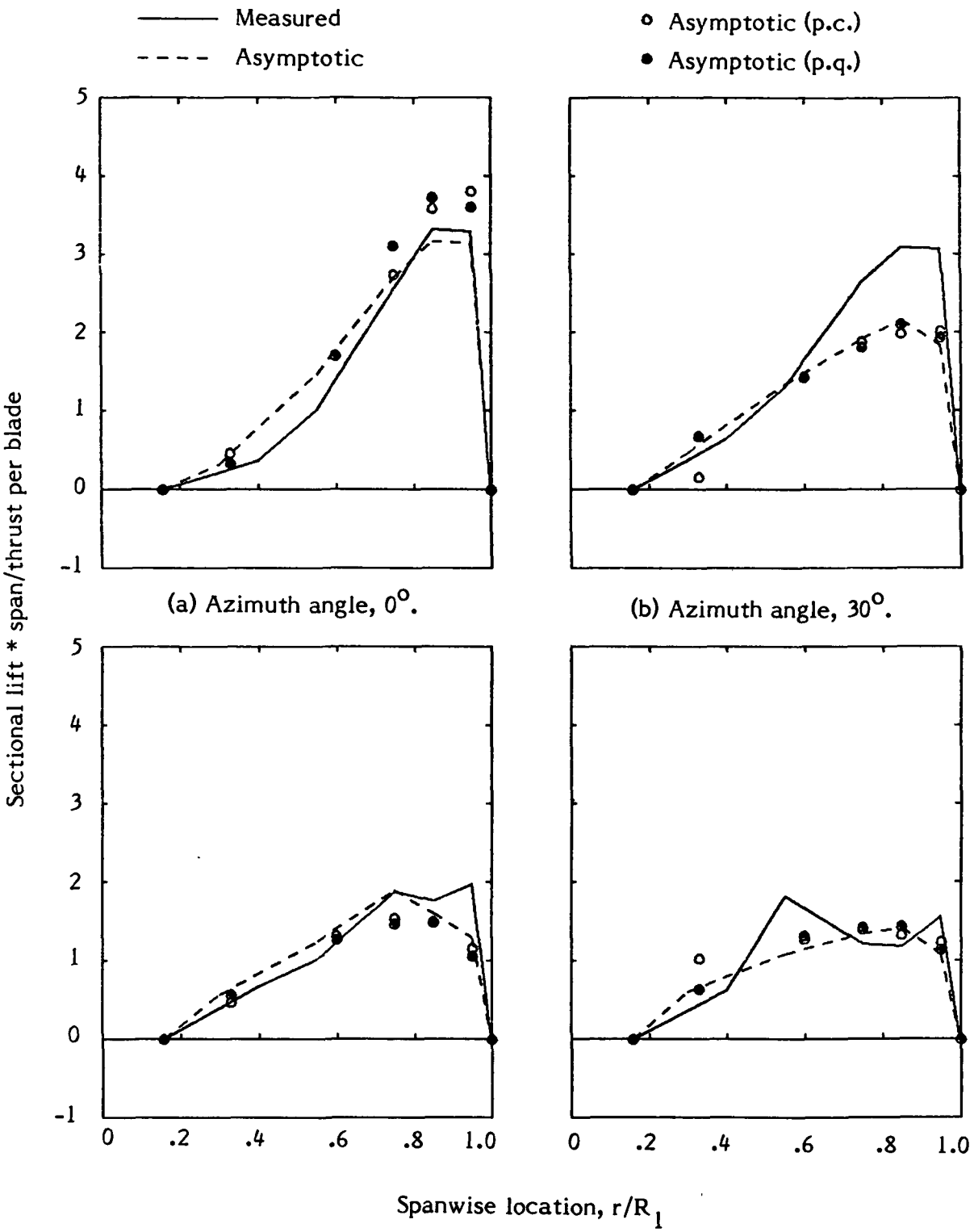

Figure 9. - Sectional lift versus spanwise location for Case 2, $\mu = 0.29$.

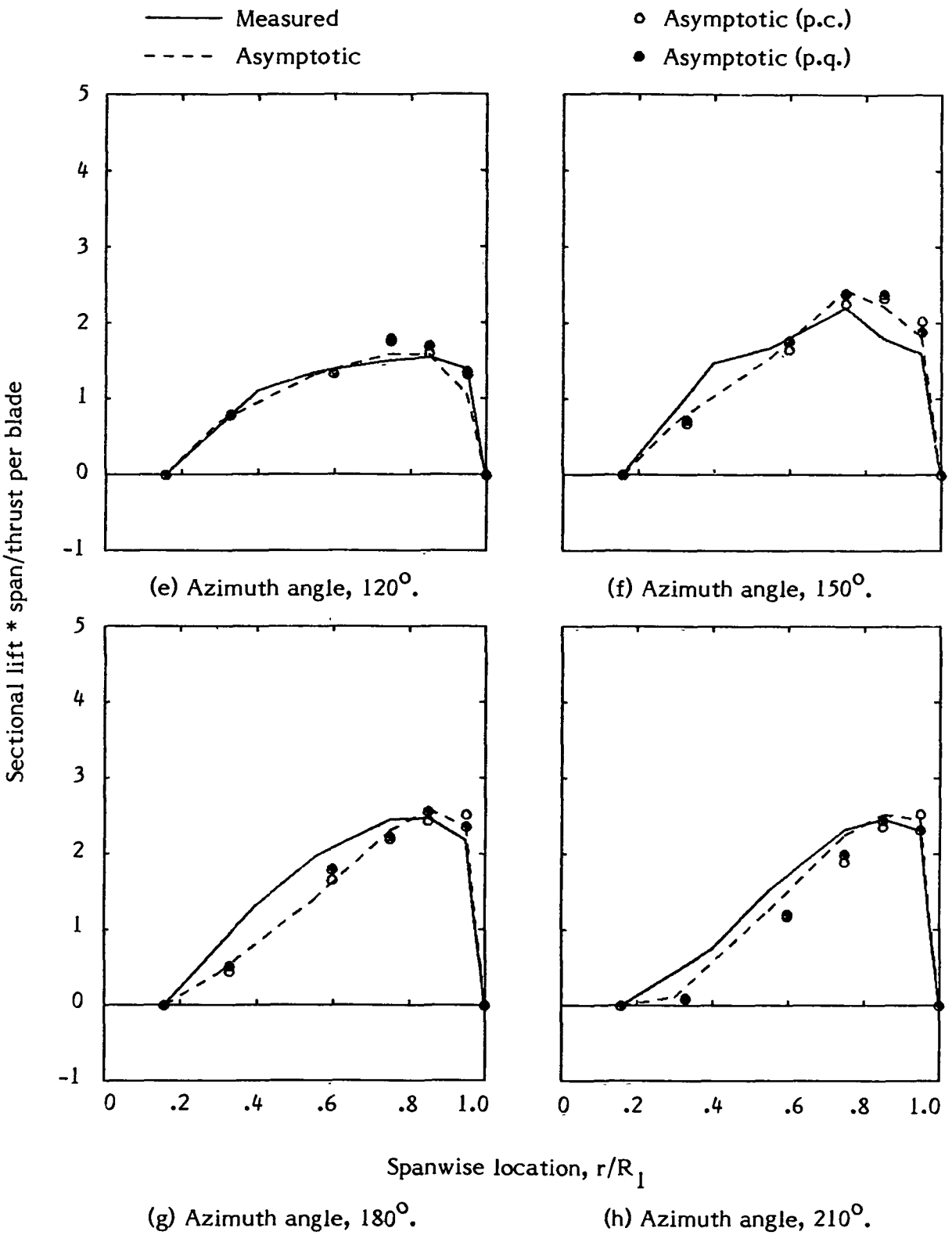

(e) Azimuth angle, 120°.

(f) Azimuth angle, 150°.

(g) Azimuth angle, 180°.

(h) Azimuth angle, 210°.

Figure 9. - Continued.

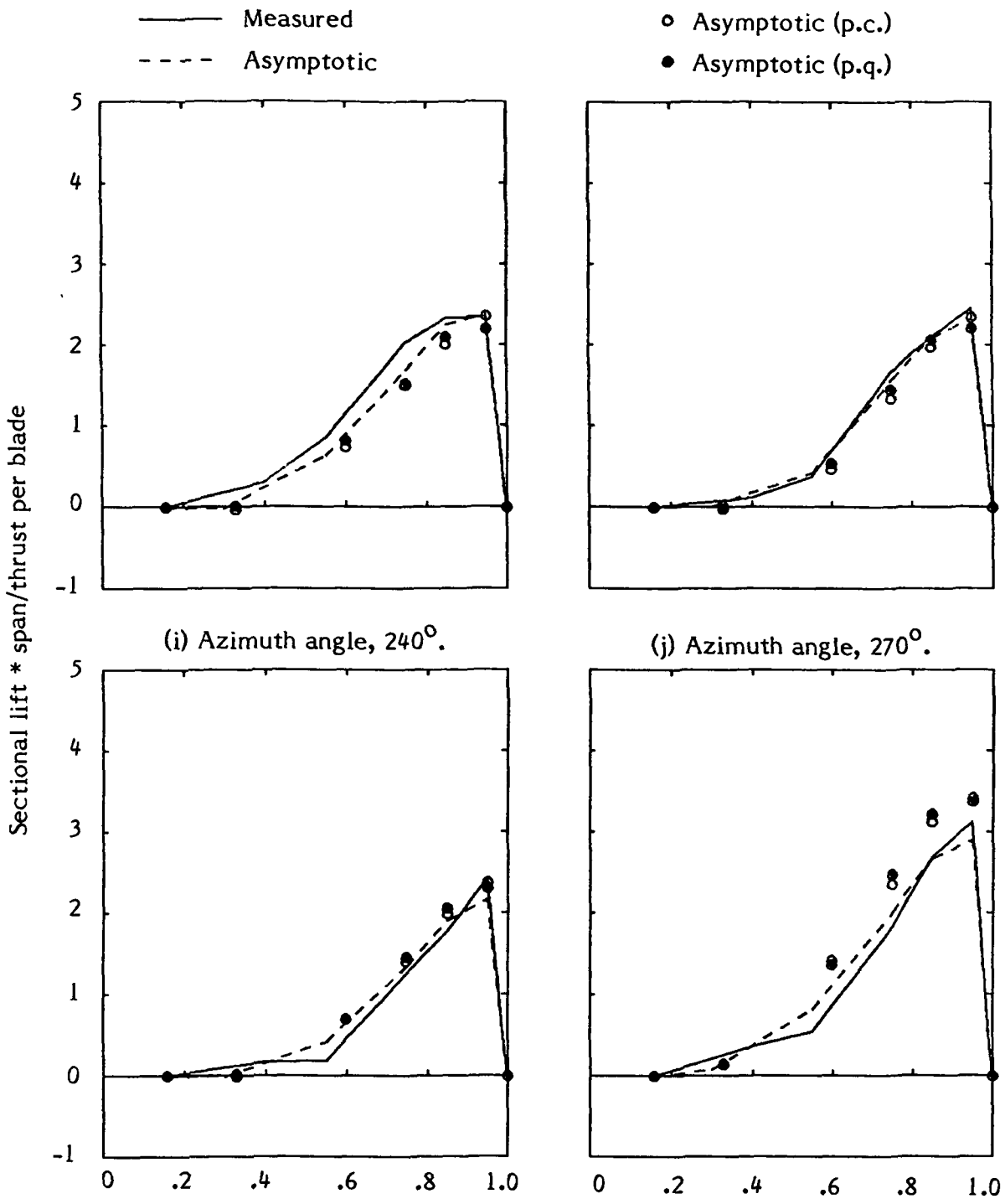

(i) Azimuth angle, 240°.

(j) Azimuth angle, 270°.

(k) Azimuth angle, 300°.

(l) Azimuth angle, 330°.

Figure 9. - Concluded.

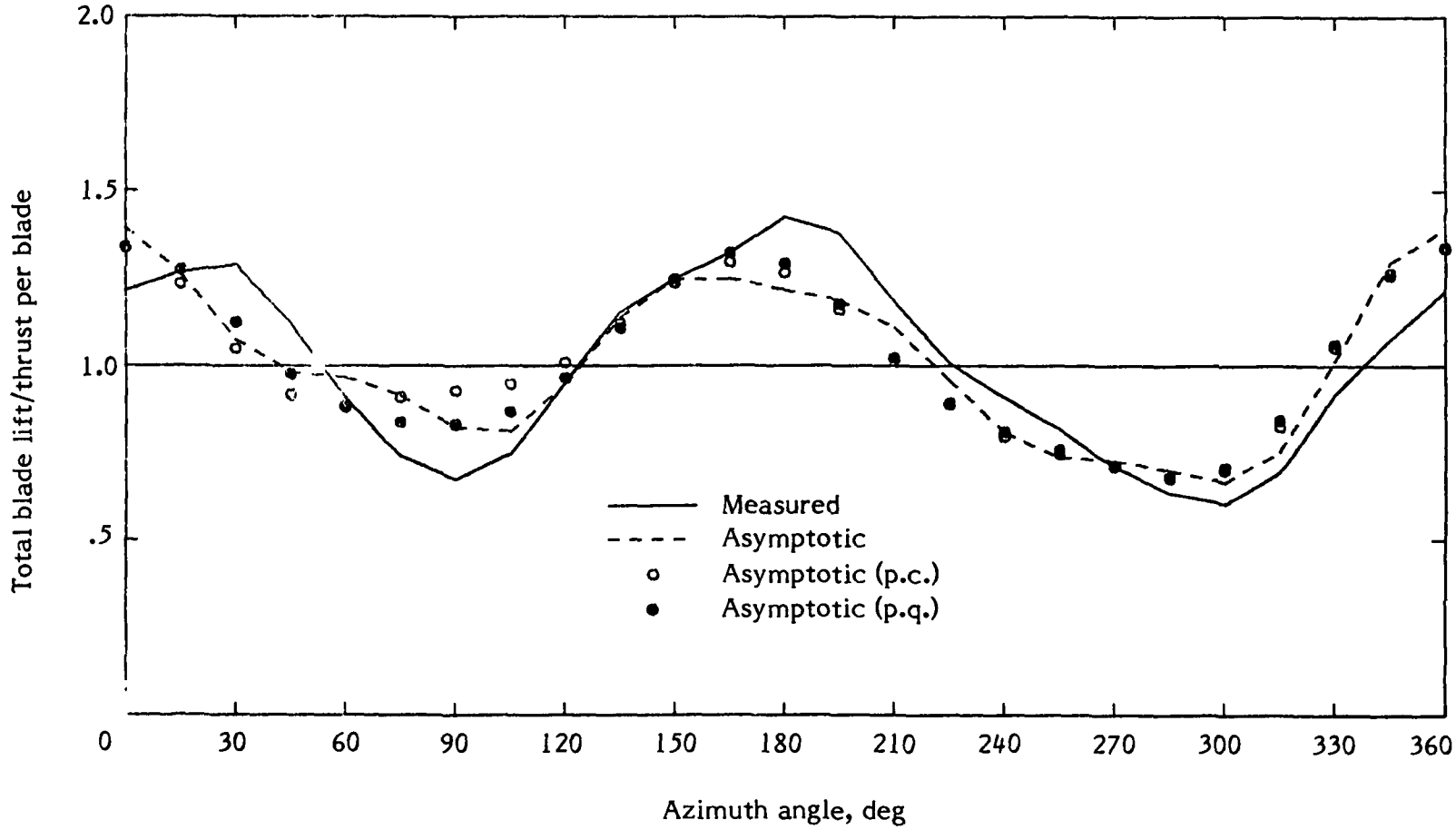

Figure 10. - Computation with constant azimuth spacing of 5^{o}, Case 2, $\mu = 0.29$.

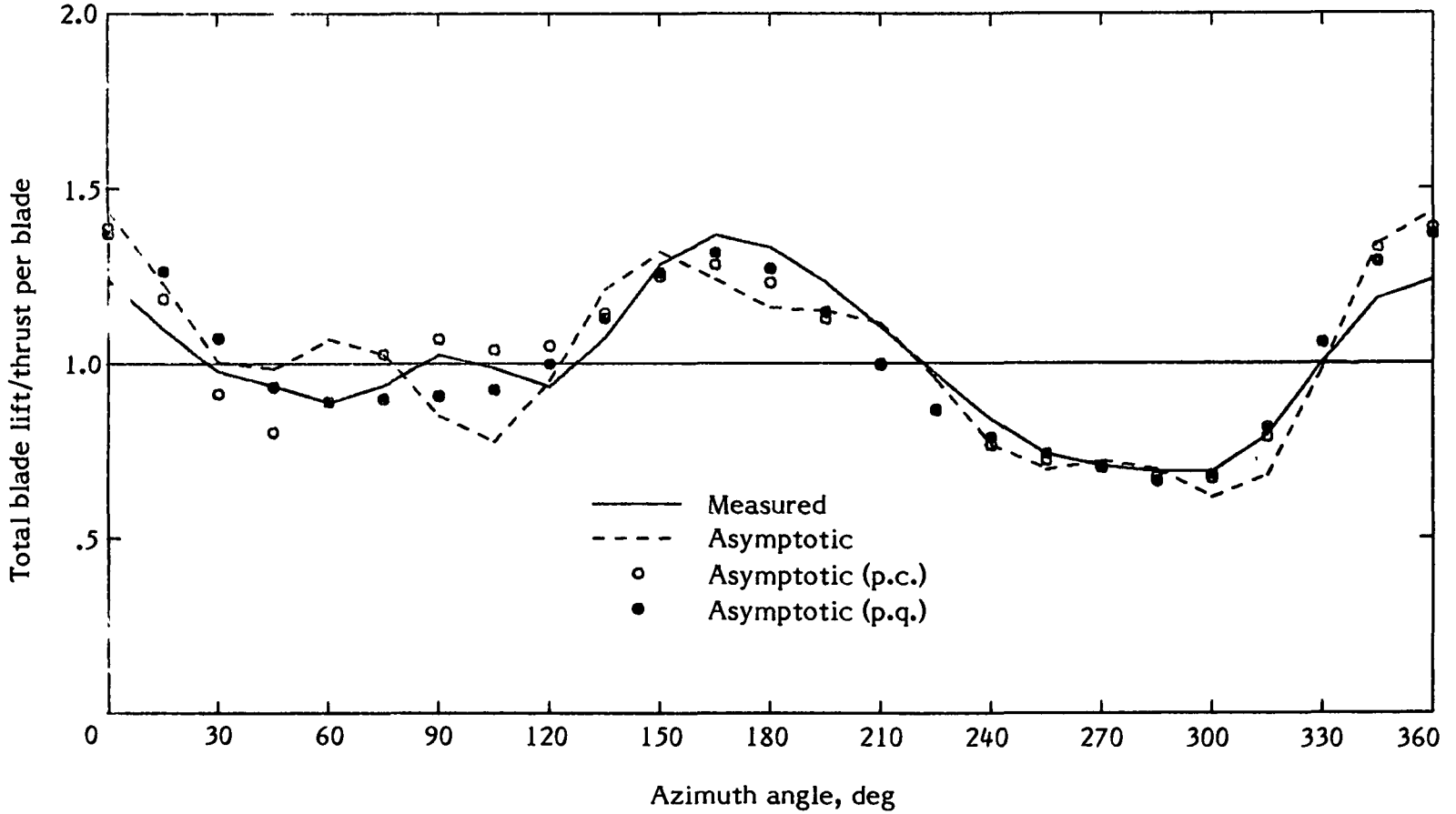

Figure 11. - Computation with constant azimuth spacing of 5°, Case 3, $\mu = 0.29$.

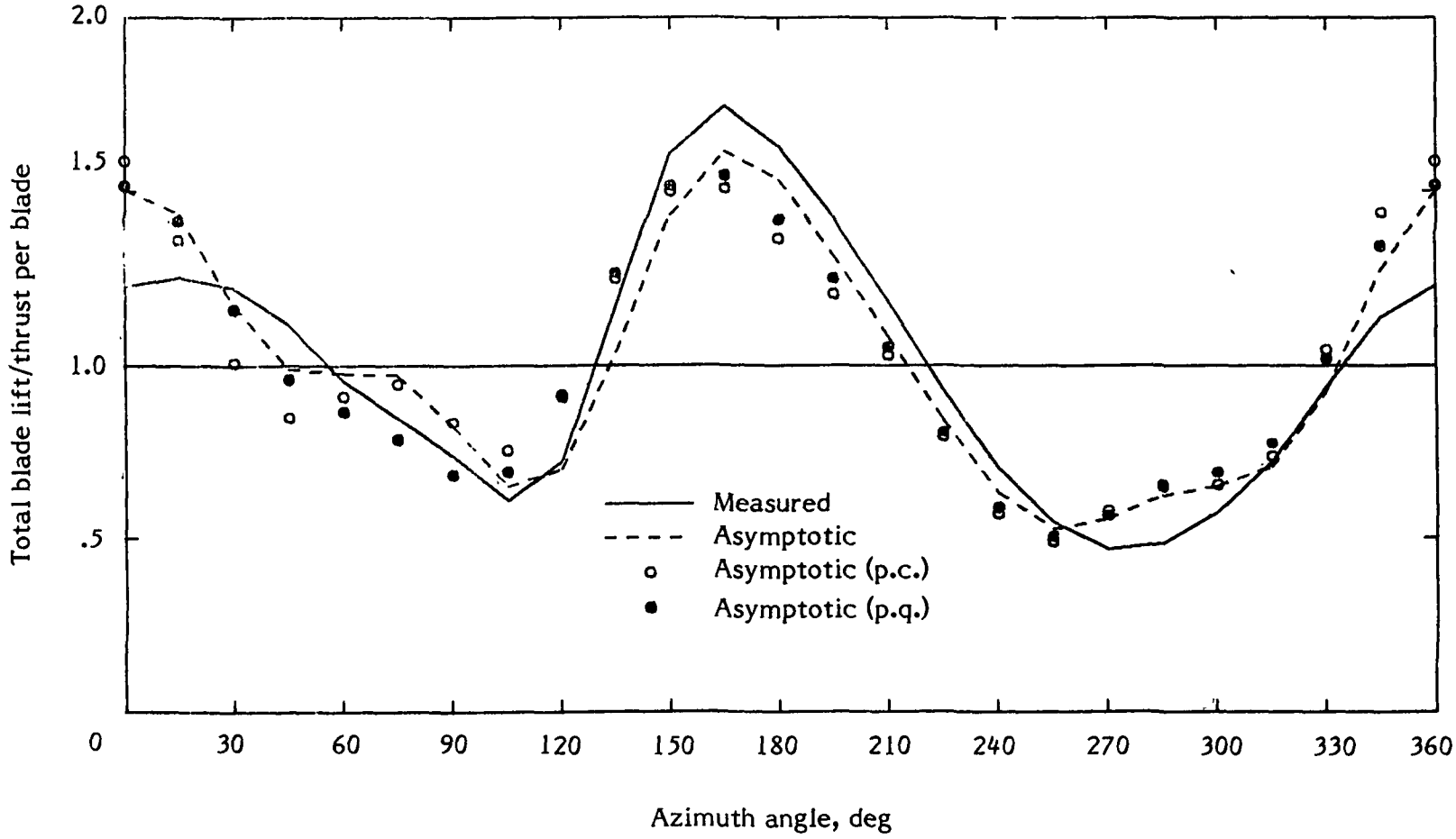

Figure 12. - Computation with constant azimuth spacing of 5^{o}, Case 3, $\mu = 0.39$.

1. Report No.	2. Government Accession No.	3. Recipient's Catalog No.
NASA CR-166092		

4. Title and Subtitle	5. Report Date
HELICOPTER ROTOR LOADS USING DISCRETIZED MATCHED ASYMPTOTIC EXPANSIONS	May 1983
	6. Performing Organization Code
7. Author(s)	8. Performing Organization Report No.
G. Alvin Pierce and Anand R. Vaidyanathan	
	10. Work Unit No.
9. Performing Organization Name and Address	
Georgia Institute of Technology School of Aerospace Engineering Atlanta, Georgia 30332	11. Contract or Grant No. NAS1-16817
	13. Type of Report and Period Covered
12 Sponsoring Agency Name and Address	Final Report
National Aeronautics and Space Administration Washington, DC 20546	14. Sponsoring Agency Code

15. Supplementary Notes

The contract research effort which led to the results in this report was financially supported by the Structures Laboratory, USARTL (AVRADCOM).
Langley Technical Monitor: John D. Berry Final Report

16. Abstract

This investigation is intended to improve the numerical practicality of a matched asymptotic expansion approach for the computation of unsteady three-dimensional airloads on a helicopter rotor. The original method as suggested by Van Holten has previously been evaluated and proven to be a comprehensive and accurate analysis for flight conditions conducive to linear flow phenomena. This effort to decrease the computational requirements of the original analysis utilizes a discretized representation of the doublet strength distribution and helical streamlines. The continuous variation of the doublet strength has been approximated by piecewise constant or piecewise quadratic distributions, and the helical trajectory of a fluid particle has been approximated by connected straight line segments. As a direct result of these simplified representations the computational time required for the execution of a typical flight condition has been reduced by an order of magnitude with respect to the requirements of the original analysis. Airloads which have been computed using the discretized method for a two-bladed model rotor and a full-scale four-bladed rotor are in close agreement with measured results and airloads from the original asymptotic analysis. For conditions characterized by significant rotor/wake interaction the piecewise constant representation requires a reduced azimuth spacing to maintain acceptable accuracy.

17 Key Words (Suggested by Author(s))	18. Distribution Statement
Unsteady airloads, Helicopter rotor, Potential flow, Asymptotic expansion	Unclassified - Unlimited Subject Category 02

19 Security Classif. (of this report)	20. Security Classif. (of this page)	21. No. of Pages	22. Price
Unclassified	Unclassified	76	